Resolution of collided ribosomes by ZNF598 is required for adipocyte energy dissipation

Toufic Kassouf[1], Laura Ryder[2], Katia El Ghoz[1], Bartosz Artur Kucharski[1], Lucile Dollet[4], Filip Dziaczkowski[1], Goda Snieckute[2], Sijie Chen[2], José Francisco Martínez[2], Dominika Malińska[1], Angel Loza-Valdes[1], Malgorzata Alicja Sliwinska[1], Eric Bennett[3], Zach Gerhart-Hines[4], Simon Bekker-Jensen[2,#], and Grzegorz Sumara[1, #]

[1]*Dioscuri center for metabolic disease, Nencki Institute of Experimental Biology, Polish Academy of Sciences, Warsaw, Poland*

[2]*Center for Gene Expression, Department of Cellular and Molecular Medicine, University of Copenhagen, Blegdamsvej 3, DK-2200 Copenhagen, Denmark*

[3]*School of Biological Sciences, Department of Cell and Developmental Biology, University of California, San Diego, La Jolla, California, USA*

[4]*Novo Nordisk Foundation Center for Basic Metabolic Research, Faculty of Health and Medical Sciences, University of Copenhagen, Blegdamsvej 3B, DK-2200 Copenhagen, Denmark;*

[#] *Correspondence should be addressed to Grzegorz Sumara (g.sumara@nencki.edu.pl) and Simon Bekker-Jensen (sbj@sund.ku.dk)*

ABSTRACT

Mitochondrial uncoupling in brown and beige adipocytes underlies non-shivering thermogenesis, during which cells exhibit elevated mitochondrial activity and protein synthesis. Here, we identify the ribosome-associated quality control (RQC) pathway, initiated by the ubiquitin ligase ZNF598, as essential for resolving translation conflicts and ribosome collisions that arise during this process. We demonstrate that β-adrenergic stimulation, cold exposure, and dietary changes induce RQC in adipocytes. ZNF598 is required for stimulated mitochondrial biogenesis, respiration, and uncoupling, and mice with adipocyte-specific *Znf598* deletion display impaired adipose browning and metabolic dysfunction when obese. Conversely, induced overexpression of ZNF598 in adipocytes of adult mice enhances RQC capacity and improves adaptive adipose responses. These findings establish translational rewiring and ribosome collision as features of thermogenesis and RQC as a critical mediation strategy.

INTRODUCTION

Adipose tissue is the central energy-storing organ that strongly influences whole-body metabolism. White adipocytes store large quantities of energy in the form of triglycerides (TG) while beige and brown adipocytes additionally dissipate energy in the form of heat. Thermal or dietary challenges can trigger various hormonal-induced signals, including β-adrenergic-dependent signaling, that drive the transition from white to beige adipocytes. In brown and beige adipocytes, β-adrenergic signaling boosts mitochondrial content and activity to sustain adaptive thermogenesis. Similarly, β-adrenergic signaling induces the expression of uncoupling protein 1 (UCP1), which disrupts the proton gradient used for ATP synthesis, resulting in energy dissipation as heat (Chouchani et al., 2019). The induction of adaptive thermogenesis in brown fat and the browning of white adipose tissue contribute to the amelioration of obesity and diabetes (Chouchani et al., 2019). Cold exposure and β-adrenergic stimuli induce, among dozens of other transcription factors, Peroxisome Proliferator-Activated Receptor-Gamma Coactivator-1 α (PGC1α) (Inagaki et al., 2016) and PR domain containing 16 (PRDM16) (Seale et al., 2008) to upregulate expression of mitochondrial genes and *UCP1* in adipocytes. The proteins encoded by these transcripts support oxidative phosphorylation and thermogenic capacity. While considerable attention has been given to transcriptional events occurring during adaptive thermogenesis, regulation at the translational level is much less studied. Consequently, the scale at which translation and ribosomal output is rewired upon hormonal and environmental cues in brown and beige adipocytes remain poorly understood. Previous studies indicate that exposure to cold or β-adrenergic stimulation enhances ribosomal output in adipocytes (Klingenspor et al., 1996) with unknown consequences for translation fidelity.

Cells have evolved a suite of surveillance pathways to detect and resolve translation conflicts. These include specific responses to stalled and collided ribosomes, which can result from

ribosomal congestion on problematic mRNA sequences, under-availability of amino acids and tRNAs, oxidative stress, or genetic mutations (Filbeck et al., 2022b; Juszkiewicz et al., 2018; Kim and Zaher, 2022). Collided ribosomes are sensed by cells as a proxy for aberrant translation and trigger ribosome-associated quality control (RQC) (Filbeck et al., 2022b; Ikeuchi et al., 2018; Kim and Zaher, 2022; Vind et al., 2020a). The RQC machinery is conserved from yeast to human cells and is related not only to cytosolic protein quality control but also to mitochondrial function and protein aggregation (Filbeck et al., 2022b; Ikeuchi et al., 2018). The unique structure of collided ribosomes is recognized by the E3 ubiquitin ligase ZNF598 that promotes ubiquitination of the ribosomal proteins uS10 (RPS20) and eS10 (RPS10) (Juszkiewicz and Hegde, 2017; Narita et al., 2022; Sundaramoorthy et al., 2017). ZNF598-ubiquitinated ribosomes accrue the RQC-trigger (RQT – ASCC2, ASCC3, and TRIP4 (Filbeck et al., 2022a; Juszkiewicz et al., 2020; Lehmann et al., 2024)) complex for resolution, thus enabling trapped nascent chains to be extracted and degraded and ribosomal subunits to be recycled (Filbeck et al., 2022b; Ikeuchi et al., 2018; Kim and Zaher, 2022; Vind et al., 2020a). Separate from ZNF598-mediated ribosome ubiquitination, the E3 ligase RNF10 ubiquitinates uS3 (RPS3) and uS5 (RPS2) to promote degradation of 40S subunits engaged in non-productive mRNA binding (initiation RQC, iRQC). These may result from ZNF598-mediated resolution of collided ribosomes, impaired 40S initiation scanning, or prolonged nutrient starvation (Lehmann et al., 2024). RNF10-mediated ubiquitination is counteracted by the deubiquitinating enzyme USP10 (Garshott et al., 2021; Garzia et al., 2021), and 40S decay requires RIOK3 engagement with ubiquitinated 40S (Coria et al., 2025; Ford et al., 2025; Huang et al., 2025). Following resolution of the leading ribosome in the collision structure, the remaining 80S ribosome is dissociated by the ribosome recycling factors Pelota, HBS1L, and ABCE1 (Filbeck et al., 2022b; Ikeuchi et al., 2018; Kim and Zaher, 2022; Vind et al., 2020a). While 40S subunits can either be directly recycled for subsequent rounds of translation or degraded through RIOK3

action, 60S subunits remain associated with peptidyl-tRNA and nascent chains. These particles are recognized by the RQC component NEMF that binds tRNA exposed at the subunit interface of 60S-nascent chain complexes. This event facilitates binding of the E3 ubiquitin ligase Listerin (LTN1), leading to ubiquitination, p97-mediated extraction, and proteasomal degradation of the nascent chain (Filbeck et al., 2022b; Ikeuchi et al., 2018; Kim and Zaher, 2022; Vind et al., 2020a).

Apart from the severe and early-onset neurodegeneration associated with *Ltn1* and *Nemf* whole-body knockout in mice (Chu et al., 2009; Martin et al., 2020), physiological contexts for ribosome collision and the importance of RQC for mammalian biology have yet to be appreciated. This includes its role in metabolism in general and in adipose tissue function, in particular. Our results highlight that adaptive thermogenesis is associated with a massive translational burst that is largely uncoupled from transcriptional gene activation. The resulting congestion of ribosomes on transcripts leads to widespread ribosome collision in adipocytes exposed to thermogenic stimulation. While RQC is dispensable for adipose tissue establishment during development, the pathway becomes critically important during adaptive responses such as white adipose tissue (WAT) browning and thermogenesis. We show that ZNF598 is required and sufficient for the induction of heat dissipation by mitochondria in brown/beige adipocytes. At the mechanistic level, ZNF598 supports the induced biogenesis of mitochondrial mass, mitochondrial proteins, and the uncoupler UCP1. Finally, conditional deletion of the *Znf598* gene in mouse adipocytes resulted in adipose tissue dysfunction and glucose intolerance, while overexpression of this factor prevented diet-induced diabetes and enhanced responses to β-adrenergic stimulation.

RESULTS

Stimulation of thermogenesis is associated with translational upregulation, ribosome collision, and induction of the RQC machinery in adipocytes

Activation of the adaptive thermogenesis program in brown and beige adipocytes by cold challenge, adrenergic stimulation, or dietary interventions requires remodeling of their subcellular structure and metabolism, incl. the acquisition of mitochondrial mass (Inagaki et al., 2016). Stimulation of murine stromal vascular cells (SVC)-derived brown adipocytes, T37i-derived murine beige/brown adipocytes, and SVC-derived white adipocytes (Fig. 1A) with the β-adrenergic agonist CL-316,243 (CL) increased ribosomal output as evidenced by incorporation of puromycin into nascent chains (Fig. 1B; Fig. S1A,B). Correlating published transcriptome and proteome datasets from BAT tissue of mice exposed to acute cold (6 hours and 8 hours, respectively), we noticed that translational induction of mitochondria-related mRNAs appeared to dominate over transcriptional changes at this early timepoint (Fig. 1C). Such upregulated translational efficiency may compromise translational fidelity and engage the RQC pathway. Cold challenge of mice for 24 hours was accompanied by transcriptional up-regulation of *Znf598* (also referred to as *Zfp598*) and most other genes encoding components of the core RQC pathway, in both BAT and inguinal white adipose tissue (iWAT) (Fig. 1D,E). Moreover, the genes encoding the three known components of iRQC (RNF10, USP10, and RIOK3) were also significantly upregulated in BAT and iWAT by cold challenge (Fig. S1C,D). Of note, expression of genes related to the ribotoxic stress and integrated stress responses (RSR and ISR) (Vind et al., 2020b) were not affected during the acute phase of the cold response in BAT and iWAT (Fig. S1C,D). This was except for the genes encoding the GCN1-associated ubiquitin ligases RNF25 and RNF14, which are also involved in quality control, specifically turnover of ribosomes with EEF1A trapped in the A-site or terminally stalled by mRNA-protein cross-links (Oltion et al., 2023; Rahmanto et al., 2023; Zhao et al., 2023) (Fig. S1C,D).

Consistent with the above *in vivo* results, β-adrenergic stimulation of SVC-derived brown and white adipocytes also enhanced the expression of *Znf598* and other RQC-related genes (Fig. 1F,G). ZNF598 protein, the rate-limiting enzyme for RQC activity (De La Cruz et al., 2025), was elevated in BAT in response to cold challenge (Fig. 1H; Fig. S1E). Moreover, the abundance of ZNF598 was robustly increased in BAT and inguinal WAT (iWAT) of mice reared on a high-fat diet (HFD) for a short or prolonged time (Fig. 1I; Fig. S1F-H).

To monitor RQC engagement in adipocytes, we stably transfected T37i cells with a stalling reporter. The expressed mRNA accrues queues of ribosomes on a string of 20 AAA-based lysine codons that separates open reading frames (ORFs) for a green and a red fluorescent protein (GFP-20K-mKate2) (modified from (Geng et al., 2024)). The underlying principle of this assay is that mKate2 synthesis (mKate2/GFP ratio) is suppressed by ZNF598-mediated removal of queuing ribosomes on the stalling sequence. Defects in RQC activity or over-engagement of the pathway due to general collision stress at endogenous transcripts can be read out as an increase in the mKate2/GFP ratio. Stimulation of differentiated T37i BAT-like cells with CL and isoproterenol (Iso) increased mKate2-to-GFP ratio (Fig. 1J,K), indicating the appearance of ZNF598-engaging ribosome collisions on endogenous transcripts upon β-adrenergic stimulation. We also examined RQC activity with a modified reporter targeting the GFP-20K-mKate2 fusion protein to mitochondria (MitoGFP-20K-mKate2), which returned a similar result (Fig. 1L). These data suggest that β-adrenergic stimulation of adipocytes engages the RQC machinery to levels that impair dissociation of ribosomes from reporter-based stall sequences, despite elevated expression of RQC components. We next employed CRISPR technology to generate T37i cells KO (knockout) for *Znf598* (*Znf598*$^{-/-}$) (Fig. S1I). In differentiated T37i, proteomic profiling of ubiquitination site abundance revealed, among others, CL-induced and ZNF598-dependent ubiquitination of relevant lysines on RPS10 (Fig.

1M; Table S1). ZNF598-dependent RPS10 ubiquitination was also induced in differentiated T37i and differentiated 3T3L1 (WAT-like adipocyte precursor) upon stimulation with β-agonist, this time determined by western blot using the ribosome inhibitor anisomycin as a positive control (Fig. 1N,O, and Fig. S1J). Of note, differentiated but unstimulated T37i, unlike 3T3L1, displayed relatively high levels of RPS10 ubiquitination when assayed by this approach. Our results indicate that ribosome collision occurs upon thermogenic stimulation in adipocytes and that upregulation of the RQC pathway is evoked as a programmed protective response for cell-adaptive purposes.

RQC is required for thermogenesis-associated enhanced translation of mitochondrial proteins and UCP1.

To investigate whether ZNF598 affects the β-adrenergic stimulation-induced translational upregulation of mitochondrial genes, we analyzed total proteome changes in differentiated WT and *Znf598*$^{-/-}$ T37i cells. Principal component analysis (PCA) hinted that the large-scale proteome reprogramming induced by CL stimulation in these cells (separation according to principal component (PC) 1) were largely ZNF598-dependent (Fig. 2A). Comparing only CL-stimulated conditions, virtually all mitochondrial proteins as wells as UCP1 were less abundant in *Znf598*$^{-/-}$ cells compared to WT, suggesting that these cells are deficient for building mitochondrial mass (Fig. 2B; Table S2). Functional enrichment of protein networks also revealed that ZNF598 loss primarily negatively affected the abundance of mitochondrial proteins (Fig. 2C). Comparison of the mock-treated conditions revealed that these ZNF598-dependent differences could even be observed in resting T37i cells (Fig. S2A,B). Western blot analysis confirmed a clear ZNF598-dependent reduction in mitochondrial respiratory chain complexes and UCP1 in these cells, both under basal, CL- and Iso-stimulated conditions (Fig. 2D,E). We also studied SVC cells derived from adipose tissue stromal vascular fraction of mice

with tamoxifen-inducible *Znf598* gene deletion ("*Znf598* cKO", genotype *Rosa26-CreERT2 ; Znf598*$^{fl/fl}$). When treated with tamoxifen and differentiated into brown adipocytes (Fig. 2F), these cells displayed modestly reduced abundance of the thermogenesis-related factors UCP1, DIO2 (Deiodinase type 2), and some respiratory chain proteins despite an incomplete targeting of the *Znf598* locus (Fig. 2G). Similar effect sizes were observed upon acute and incomplete knockdown of ZNF598 in T37i cells by siRNA (Fig. 2H). These differences in protein abundance were not mirrored by lower levels of mRNAs encoding mitochondrial proteins and thermogenesis-related factors. Rather, these mRNAs were enhanced in SVC-derived ZNF598-deficient brown adipocytes (Fig. S2C). In addition to their function in thermogenesis, white, beige, and brown adipocytes serve as dynamic energy repositories for the organism. Feeding, fasting, and energy demand in the periphery define the rate of lipid synthesis and degradation. Deletion of *Znf598* in T37i and differentiation into the BAT-like state did not affect the abundance of major proteins involved in lipogenesis (ACC and FASN), triglyceride synthesis (DGAT), fatty acid transport (CD36), or lipolysis (ATGL, HSL, and pHSL) under basal or β-adrenergic stimulated conditions (Fig. S2D). These results indicate that ZNF598 specifically regulates the translation of thermogenesis-related proteins without affecting unrelated aspects of adipocyte biology.

ZNF598 is required for mitochondrial biogenesis and function in brown and beige adipocytes

All of the above indicate that RQC is required for mitochondrial function in adipocytes with thermogenic capacity. Indeed, ZNF598-deficient brown adipocytes were impaired in both basal respiration and maximal mitochondrial capacity, regardless of whether they originated from *Znf598* KO or *Znf598* siRNA-treated T37i cells or from SVC-derived ZNF598-deficient precursor cells, as measured by oxygen consumption rate by Seahorse technology (Fig. 3A,B;

Fig. S3A). Moreover, T37i-derived brown adipocytes deleted for *Znf598* were refractory to β-agonist-induced boosting of the same parameters (Fig. 3C). Even 3T3L1-derived white adipocytes depleted for ZNF598 were refractory to the marginal boosting effects of β-agonist on mitochondrial function and abundance, but these cells did not display any differences under unstimulated conditions (Fig. S3B,C). All of these prompted us to investigate the impact of ZNF598 on mitochondrial acquisition upon β-adrenergic challenge. In SVC-derived brown adipocytes, deletion of *Znf598* blunted CL-induced increase in mitochondrial content, as indicated by mitotracker staining (Fig. 3D,E). siRNA-mediated depletion of ZNF598 in T37i-derived brown adipocytes resulted in a similar defect after challenge with two independent β-agonists, as indicated by both mitotracker staining and ratios of mitochondrial to genomic DNA (Fig. 3F-H).

Brown adipocytes display higher mitochondrial content and respiration rate compared to white adipocytes. Of note, we detected the presence of ubiquitinated species of ZNF598 and RPS10 in SVC-derived brown (but not white) adipocytes (Fig. S3D,E), indicating that the RQC pathway is active in these cells. Consistently, unstimulated SVC-derived white adipocytes deleted for *Znf598* were not negatively affected with regard to mitochondrial respiration and abundance of mitochondrial complexes (Fig. S3F,G). Taken together, ZNF598 promotes mitochondrial biogenesis and function in brown, but not white, adipocytes at basal conditions. However, the RQC machinery is required for β-adrenergic-induced mitochondrial acquisition in both.

Overexpression of ZNF598 boosts mitochondrial content, function, and uncoupling activity.

ZNF598 was recently demonstrated to be a rate-limiting factor for RQC activity (De La Cruz et al., 2025). Overexpression of ZNF598 in T37i-derived brown adipocytes was sufficient to elevate mitochondrial to genomic DNA ratio (Fig. S4A) and increase basal respiration, uncoupling activity, and maximal respiratory capacity of mitochondria (Fig. 4A). Electron microscopy-based analyses of the ultrastructure of these cells revealed an increased number and reduced size of mitochondria, especially those in contact with lipid droplets (Fig. 4B,C; Fig. S4B). These effects were accompanied by increased levels of respiratory complexes and elevated levels of UCP1 in ZNF598-overexpressing cells (Fig. 4D). As a likely consequence of the higher numbers of mitochondria, these cells also displayed lower levels of triglycerides (Fig. S4C,D). We also generated SVC-derived brown adipocytes with Tamoxifen-induced overexpression of ZNF598 (mouse genotype *Adipoq*^{CreERT2}; *Rosa26*$^{LSL\text{-}Flag\text{-}Znf598}$, alias *Znf598*$^{Adipoq\text{-}OE}$). When induced by tamoxifen prior to differentiation (Fig. 4E), these cells displayed elevated basal respiration, increased uncoupling activity, maximal respiratory capacity, increased abundance of UCP1 and respiratory complexes, and elevated mitochondrial to genomic DNA ratio and mitotracker signals (Fig. 4F,G; Fig. S4E), all indicators of increased mitochondrial mass and thermogenic activity. The effects of ZNF598 overexpression in T37i brown adipocytes were not further enhanced by β-adrenergic stimulation (Fig. 4H-J) and were not associated with changes in abundance of proteins involved in lipogenesis, triglyceride synthesis, lipid transport, and lipolysis (Fig. S4F). ZNF598 overexpression in SVC-derived brown adipocytes was also not associated with major changes in expression of the underlying genes (Fig. S4G). Finally, when overexpressed in SVC-derived white adipocytes, ZNF598 also had mild positive effects on basal respiration, uncoupling activity, and mitochondrial content (Fig. S4H-J) independent of effects on gene expression (Fig. S4K). Altogether, our results indicate that RQC activity can be boosted by overexpression of ZNF598 in brown adipocytes with positive effects on mitochondrial content, respiratory capacity, and uncoupling activity

even in the absence of hormonal stimulation. This concept is on par with ZNF598, recently being described as a rate-limiting factor for RQC activity (De La Cruz et al., 2025).

Knockout of *Znf598* in adipocytes suppresses inducible iWAT browning and promotes glucose intolerance in mice.

To study the effects of RQC in adipocytes *in vivo*, we generated mice carrying a conditional allele of *Znf598* (*Znf598*-flox). Excision of LoxP sites in *Znf598*-flox crossed with adipocyte-specific CRE-expressing mice (*Adipoq-cre*) resulted in the deletion of exons 2 to 5 ($Znf598^{adipoq\text{-}cKO}$) (Fig. S5A) and a strong decrease of *Znf598* transcript levels in white and brown adipose tissues, but not in unrelated organs such as liver (Fig. S5B). These mice appeared phenotypically normal and were indistinguishable from their WT littermates with respect to weight and adipose tissue morphology. In order to gauge the plasticity of adipocytes *in vivo*, we injected mice with β-agonist CL over 10 days and examined iWAT for inducible browning (Fig. 5A). This response, determined as the appearance of multilocular adipocytes, was markedly suppressed in $Znf598^{adipoq\text{-}cKO}$ mice (Fig. 5B,C). On the other hand, BAT tissue appeared morphologically similar between genotypes (Fig. S5C). The apparent deficiency in the CL-induced browning response was accompanied by a similar negative effect on UCP1 upregulation and a reduction in the abundance of respiratory chain complexes, in iWAT but not BAT (Fig. 5D-G; Fig. S5D-F). Consistent with our *in vitro* data, these effects were not mirrored by differences in *Ucp1* mRNA levels (Fig. S5G,H), suggesting that CL-induced iWAT browning requires translation surveillance by the RQC pathway. The effects were not attributable to differences in whole-body and adipose tissue weights between genotypes in the experiment (Fig. S5I-L).

Reduction in mitochondrial content in adipose tissue and diminished UCP1 abundance can predispose to metabolic disorders, including diabetes (Chouchani et al., 2019). To evaluate whether *Znf598*$^{adipoq\text{-}cKO}$ mice were metabolically compromised in other aspects, we subjected mice to a high-fat diet (HFD), which induces obesity and glucose intolerance (Fig. 5H). Body weight gain, food intake, and energy expenditure were similar between genotypes during the feeding regimen (Fig. S5M-O), and we also did not observe any differences in organ weights and appearances at termination. However, when subjected to a glucose tolerance test (GTT), HFD-fed *Znf598*$^{adipoq\text{-}cKO}$ mice displayed both elevated basal blood glucose levels and defective glucose clearance (Fig. 5I,J). While not impacting on the development or morphological appearance of adipose tissue, our data indicate that *Znf598* deletion and loss of RQC activity in adipocytes compromise metabolic transitions in mice, here exemplified by inducible iWAT browning and blood glucose control.

A mouse model with elevated ZNF598 expression in adipocytes displays increased thermogenic potential and improves glucose tolerance.

To further investigate the influence on the RQC pathway on adipose tissue processes *in vivo*, we generated a mouse model with inducible and adipocyte-specific ZNF598 overexpression (*Znf598*$^{Adipoq\text{-}OE}$) (Fig. S6A). Administration of tamoxifen to these mice resulted in a marked elevation of ZNF598 levels in adipose tissue (Fig. S6B). Subsequent injection of these mice with CL for 10 consecutive days (Fig. 6A) resulted in the expected decrease in body weight for both ZNF598-overexpressing and control mice without affecting food intake (Fig. S6C,D). However, *Znf598*$^{Adipoq\text{-}OE}$ mice displayed elevated energy dissipation throughout the experiment, reaching significance at day 9 of the injections (Fig. 6B). Moreover, overexpression of ZNF598 caused significant remodeling of the adipose tissue, where *Znf598*$^{Adipoq\text{-}OE}$ mice presented elevated BAT mass and a lower mass of epididymal WAT (eWAT) (Fig. 6C-E).

These differences were associated with increased browning of iWAT in *Znf598*$^{Adipoq\text{-}OE}$ mice compared to controls, as determined by the number of multilocular adipocytes in this tissue (Fig. 6F,G). While BAT architecture was not influenced by *Znf598* overexpression (Fig. 6H), UCP1 abundance was elevated in both iWAT and BAT in these mice (Fig. 6I-L). These data indicate that elevation of RQC activity is sufficient to elevate energy expenditure in mice and to potentiate the impact of β-adrenergic stimulation on thermogenesis and iWAT browning.

We also subjected this mouse strain to an obesogenic diet and evaluated the metabolic consequences (Fig. 6M). Injection of tamoxifen initially after 2 weeks of HFD resulted in lower HFD-induced weight gain in ZNF598-overexpressing mice, but this difference compared to control animals disappeared over time (Fig. S6E). Mice were given a second boost of tamoxifen injection after 8 weeks and euthanized after 13 weeks of HFD feeding (Fig. 6M). While overexpression of ZNF598 in adipocytes did not significantly alter food intake, energy dissipation, or body composition (Fig. S6F-H), HFD-fed *Znf598*$^{Adipoq\text{-}OE}$ mice displayed improved blood glucose control after GTT challenge (Fig. 6N). Taken together, overexpression of ZNF598 in adipocytes protects against HFD-induced metabolic deterioration, resulting in an opposite phenotype to *Znf598*$^{Adipoq\text{-}cKO}$ mice.

DISCUSSION

Our results highlight that activation of the thermogenic program in adipocytes is associated with a remarkable induction of translational activity and ensuing ribosome collision. As a supportive part of this program, ZNF598 and a host of other RQC pathway components are induced to mitigate the potentially deleterious effects of ribosomal congestion on mitochondrial protein-encoding mRNAs and other relevant transcripts. Consequently, interference with the RQC pathway in several *in vitro* and *in vivo* models of adaptive thermogenesis is associated

with defective cell and tissue responses. These include the acquisition of mitochondrial mass and induced iWAT browning.

Genetic defects in the RQC system are associated with neurodegenerative and neuronal disease in mice and humans (McGirr et al., 2025). Whether ribosome collision occurs on a large scale at basal conditions in other tissues or whether they manifest during physiologically relevant processes have not been appreciated. Here, we report for the first time both a physiological relevance of ribosome collision and a direct role of the RQC pathway in an extra-neuronal tissue. Our findings imply that activation of RQC is not only required for the induction of mitochondrial function and uncoupling activity in adipocytes but is also sufficient to drive these processes by selective stimulation of translation of mitochondrial proteins and UCP1. Our discoveries highlight RQC as a biological process that can be modulated to induce adaptive thermogenesis and combat obesity and associated diseases. A similar selective requirement for RQC was recently reported for human induced pluripotent stem cells (iPSCs). RQC is not required for maintenance of the pluripotent state but becomes critically important during differentiation (Rodschinka et al., 2025), which is likely associated with similar translation rewiring as in adipocytes undergoing thermogenic activation. Also, in intestinal stem cell differentiation, the metabolic shift from glycolysis to oxidative phosphorylation is brought about not by changes in gene expression but by rewiring of translational efficiency of the underlying transcripts (Silva et al., 2022). This is also the case upon T cell activation, where the inverse metabolic shift is largely regulated at the translational rather than the transcriptional level (Chang et al., 2013). Whether these two cases of translationally regulated rapid changes to cellular identity are also associated with the induction of ribosome collision and a requirement for RQC remains to be studied.

Biochemical studies have indicated that the stoichiometry of RQC pathway components relative to translation initiation and elongation factors is highly unbalanced, with RQC components being significantly less abundant (D'Orazio and Green, 2021; Monaghan et al., 2023). Our data highlight how β-adrenergic stimulation or dietary intervention increases the abundance of ZNF598 and other RQC components in adipocytes. However, as indicated by the higher rate of read-through of the stall sequence in an RQC reporter during β-adrenergic stimulation (Fig. 1J, L), the abundance of RQC components is not sufficient during the activation of the thermogenic activity of adipocytes. Previous studies indicated that engagement of the RQC pathway is critical in connection with mitochondrial stress (Geng et al., 2024). Our data from a range of *in vitro* and *in vivo* model systems highlights one physiological context where such perturbations occur and where RQC becomes critical. Deletion or silencing of *Znf598* resulted in defective upregulation of mitochondrial content and UCP1 abundance, without affecting the transcriptional induction of the underlying genes. Of note, mass spectrometry revealed UCP1 protein to be dramatically down-regulated in the absence of ZNF598 in T37i-derived brown adipocyte-like cells. While the reduced abundance of this protein might simply reflect the overall requirement of RQC for mitigating the damaging effects of rapid translational induction, it could also suggest the existence of a regulatory mechanism that directly affects the cellular production of UCP1 and mitochondrial proteins. ZNF598 is both sufficient and required for upregulation of UCP1 and mitochondrial proteins in both brown and white adipocytes.

In conclusion, our data highlight translational regulation as a key aspect of adaptive thermogenesis and demonstrate that ribosome collision is a bottleneck for the associated cellular remodeling. RQC and potentially other translation surveillance systems consequently become critical for translation of the key components determining the respiratory and thermogenic

capacity of beige and brown adipocytes. These associations may have wider implications for physiologically relevant cellular transitions that require rapid remodeling of the proteome.

ACKNOWLEDGEMENTS

We thank Drs. Malgorzata Alicja Sliwinska and Hanna Nieznańska from the Laboratory of Imaging Tissue Structure and Function for providing Transmission Electron Microscopy service, and Dr. Jedrzej Szymanski from the Laboratory of Imaging Tissue Structure and Function (both located at the Nencki Institute for Experimental Biology) for help with imaging of adipocytes. This study was supported by the Dioscuri Center of Scientific Excellence (grant number UMO-2018/01/H/NZ4/00002) – the programme initiated by the Max Planck Society (MPG), jointly managed with the National Science Center in Poland (NCN), and mutually funded by the Polish Ministry of Science and Higher Education (MNSW) and the German Federal Ministry of Research, Technology, and Space (BMFTR) granted to Grzegorz Sumara. Some of the initial results were obtained with the support of a Minatura pre-grant from the NCN (nr. 2022/06/X/NZ3/00539) awarded to Toufic Kassouf. Work in the Bekker-Jensen lab was supported by the European Research Council (ERC) under the European Union's Horizon 2020 research and innovation program (grant agreement 863911 - PHYRIST) and Independent Research Fund Denmark (grant no. 3101-00344B). Center for Gene Expression (CGEN) is a Center of Excellence funded by The National Danish Research Foundation (grant no. DNRF166). Mass spectrometry-based proteomics analyses were performed by the Proteomics Research Infrastructure (PRI) at the University of Copenhagen (UCPH), supported by the Novo Nordisk Foundation (NNF) (grant agreement number NNF19SA0059305).

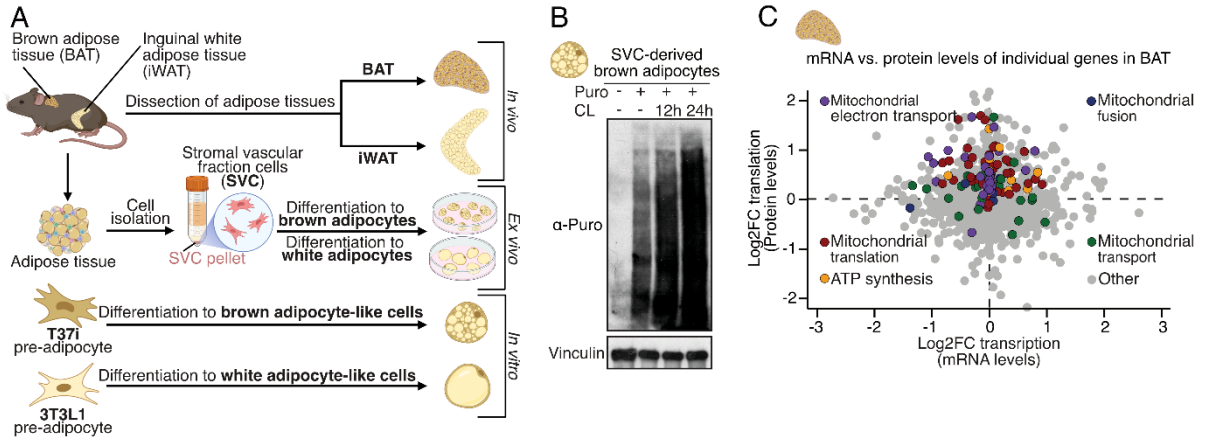

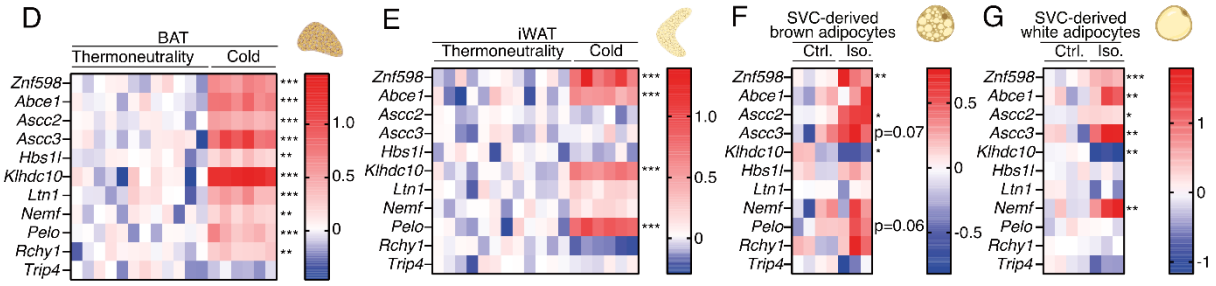

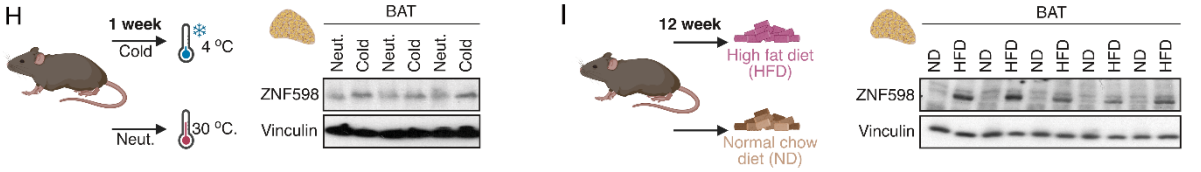

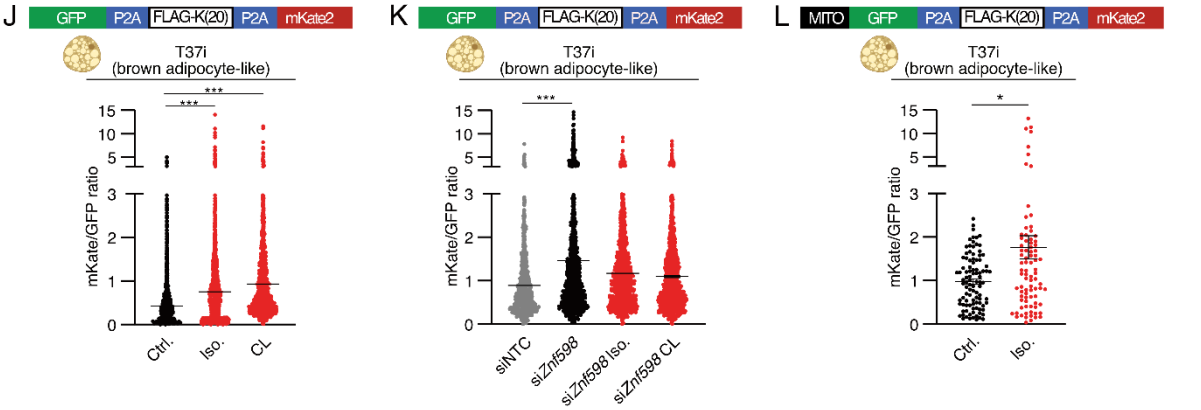

M **CL-stimulated T37i**

Protein ubiquitination sites	Log2FC	p-value
Myo1c ~ K1047	-8.4512	7.94E-06
Itga5 ~ K1042	-7.3616	0.000317
Acsl1 ~ K357	-6.72534	0.00051
Tecr ~ K67	-6.50571	6.42E-05
Stat1 ~ K658	-6.36365	0.001204
Ca3 ~ K171	-6.25142	0.000417
Rps10 ~ K138 + K139	-6.13489	0.000288
Miga2 ~ K327	-5.99694	6.02E-05
Ahnak ~ K184	-5.99144	0.000256
Cyp51a1 ~ K156	-5.9385	5.66E-05

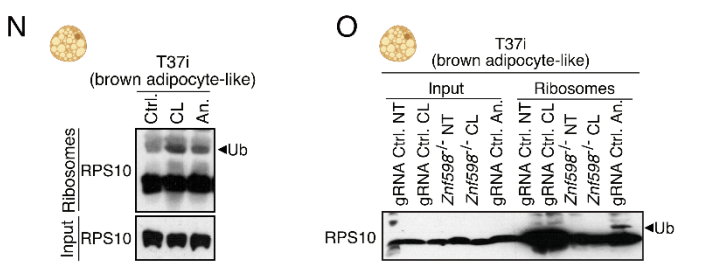

FIGURE 1. Translational Activation and Ribosome Quality Control in Thermogenic Adipocytes

(A) Experimental sources of mouse adipose tissue and adipocytes for this study. Whole brown (BAT) and white (WAT) adipose tissues were dissected from mice, stromal vascular cells (SVC) were isolated from mouse adipose tissue (white or brown) and differentiated into either brown or white adipocytes, and immortalized T37i and 3T3L1 pre-adipocyte cell lines were differentiated into brown and white adipocyte-like cells, respectively.

(B) Determination of ribosomal output using puromycin-labeling of proteins in brown adipocytes derived from SVCs treated with CL-316,243 (CL) for the indicated time.

(C) Correlation plot for mRNA vs. protein levels of individual genes in BAT of mice exposed for 6 (mRNA) and 8 (protein) hours to 4 ºC. Genes and corresponding proteins associated with the indicated processes are shown with the following colors: mitochondrial electron transport chain (GO:0022904, "respiratory electron transport chain") – purple, mitochondrial fusion (GO:0008053) – blue, mitochondrial translation (GO:0032543) – red, ATP synthesis (GO:0015986, "proton motive force-driven ATP synthesis") – orange, mitochondrial transport (GO:1990542, "mitochondrial transmembrane transport") – green, others – gray.

(D-G) Heat maps showing the log2-transformed fold changes of *Znf598* mRNA levels and mRNA levels for other components of the RQC machinery in BAT **(D)** and iWAT **(E)** of mice kept at room temperature or exposed to 4 °C (n = 12 and n = 6 biological replicates, respectively) for 24 hours, as well as in SVC-derived brown **(F)** and white **(G)** adipocytes following β-adrenergic stimulation (isoproterenol – Iso.) for 6 hours (n = 3-4 biological replicates).

(H) Western blot (WB) analysis of the abundance of ZNF598 in BAT collected from wild-type (WT) mice following 1 week of thermoneutrality (30 °C, neut.) or cold exposure (4 °C, cold).

(I) WB analysis of the abundance of ZNF598 in BAT of WT mice fed a normal chow diet (ND) or a high-fat diet (HFD) for 12 weeks.

(J) and (K) Top: schematic of a dual-fluorescent GFP-20K-mKate2 construct. GFP and mKate2 cDNA is split by a ribosomal stalling sequence containing 20 consecutive lysine (AAA) codons preceded by FLAG-tag cDNA. Bottom: Quantification of GFP to mKate2 ratio in BAT-differentiated T37i cells stably expressing the reporter and transfected with the indicated siRNAs (NTC, non-targeting control) and treated with Iso. and CL for 24 hours. Value from individual aggregates (GFP and/or mKate) from at least 10 randomly selected fields (5-8 cells per field) of view per sample are plotted, and lines indicate the mean values +/- standard error of the mean (SEM).

(L) Top: Schematic of a dual-fluorescent GFP-20K-mKate2 stalling reporter with N-terminal mitochondrial targeting signal (MITO). Bottom: Quantification of GFP to mKate2 ratio in BAT-differentiated T37i cells stably expressing the reporter and treated with Iso. for 24 hours. Values from individual cells are plotted, and lines indicate the mean values +/- SEM.

(M) Ubiquitination sites most affected by CL-treatment (24 hours – mock divided by CL, n = 3 biological replicates) of T37i brown adipocytes knockout (KO) for *Znf598* (enrichment of diGly remnant on peptides after trypsin digestion). The ZNF598-dependent and RQC-related ubiquitination sites on RPS10 are highlighted in red.

(N and O) Western blot (WB) analysis of protein lysates (input) and pelleted ribosomes from T37i brown adipocytes WT (gRNA Ctrl.) or KO ($^{-/-}$) for *Znf598*. Differentiated cells were treated with CL (24 hours) or anisomycin (An., 1 hour) as a positive control.

(D-G, M) statistical analysis was performed using DESeq2 (v. 1.34), *, p≤0.05; **, p≤0.01; ***, p≤0.001 in Wald test. (J-L) *, p≤0.05; **, p≤0.01; ***, p≤0.001 in Mann-Whitney test or student's t-test.

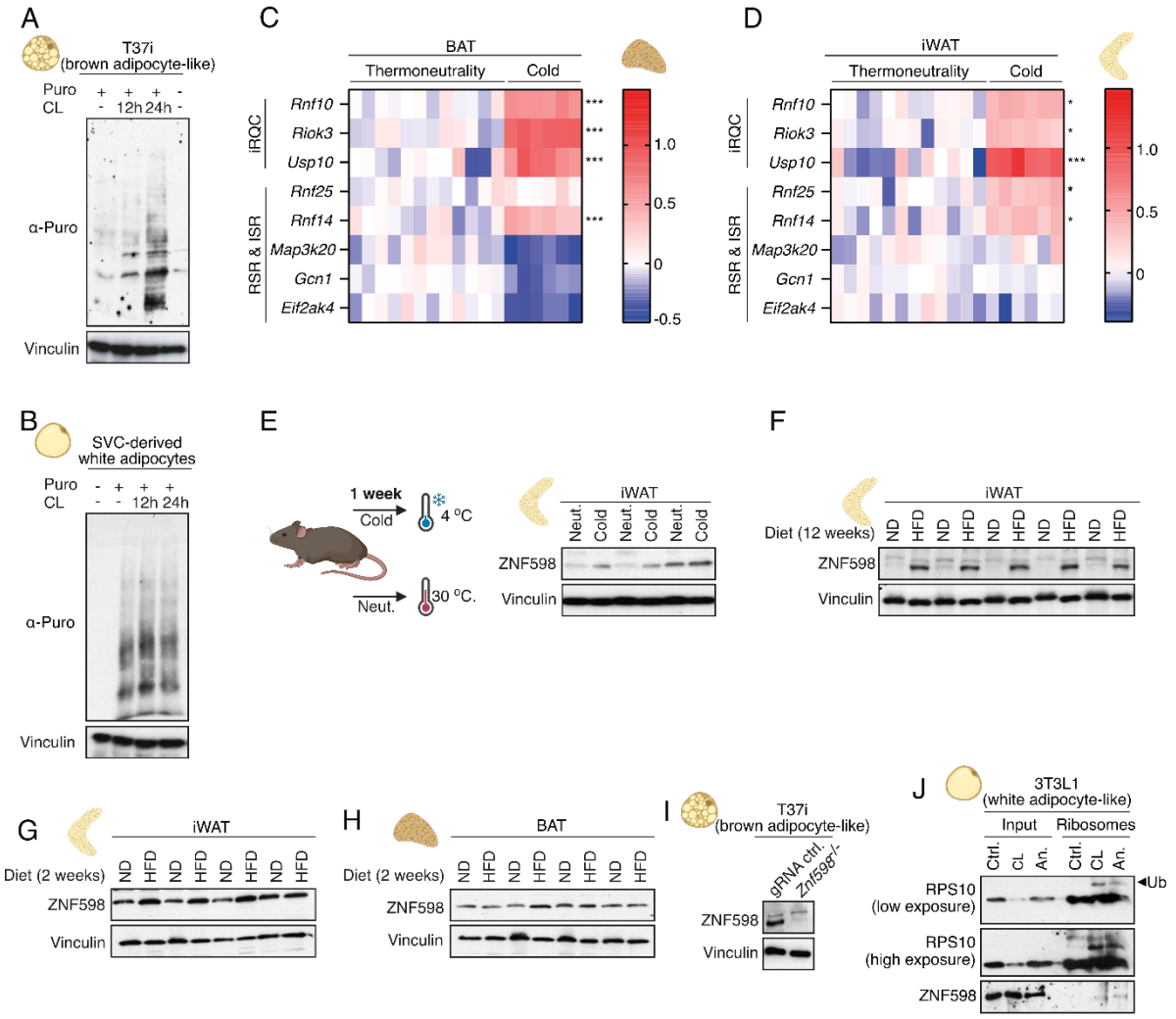

FIGURE S1. Translational Activation and Ribosome Collision in Thermogenic Adipocytes

(A-B) Determination of ribosomal output using puromycin-labeling of proteins in brown adipocytes derived from T37i cells **(A)** and white adipocytes derived from stromal vascular cells (SVC) **(B)** treated with CL-316,243 (CL) for the indicated time.

(C-D) Heat maps showing the log2-transformed fold changes of mRNA levels for proteins functioning in initiation ribosome-associated quality control (iRQC), ribotoxic stress response

(RSR) and integrated stress response (ISR) in brown adipose tissue (BAT) **(C)** and inguinal white adipose tissue (iWAT) **(D)** of mice kept at room temperature or exposed to 4 °C (n = 12 and n = 6 biological replicates, respectively) for 24 hours.

(E) Western blot (WB) analysis of the abundance of ZNF598 in iWAT collected from WT mice following 1 week of thermoneutrality (30 °C, neut.) or cold exposure (4 °C, cold).

(F) WB analysis of the abundance of ZNF598 in iWAT of WT mice fed a normal chow diet (ND) or a high-fat diet (HFD) for 12 weeks.

(G-H) WB analysis of the abundance of ZNF598 in iWAT **(G)** and BAT **(H)** of mice fed ND or HFD for 2 weeks.

(I) WB analysis of the abundance of ZNF598 in WT (gRNA Ctrl.) and *Znf598* knockout ($^{-/-}$) T37i cells.

(J) Western blot (WB) analysis of protein lysates (input) and pelleted ribosomes from 3T3L1 adipocytes treated with CL (24 hours) or anisomycin (An, 1 hour) as a positive control.

(C, D) *, $p \leq 0.05$; ***, $p \leq 0.001$ in student's t-test.

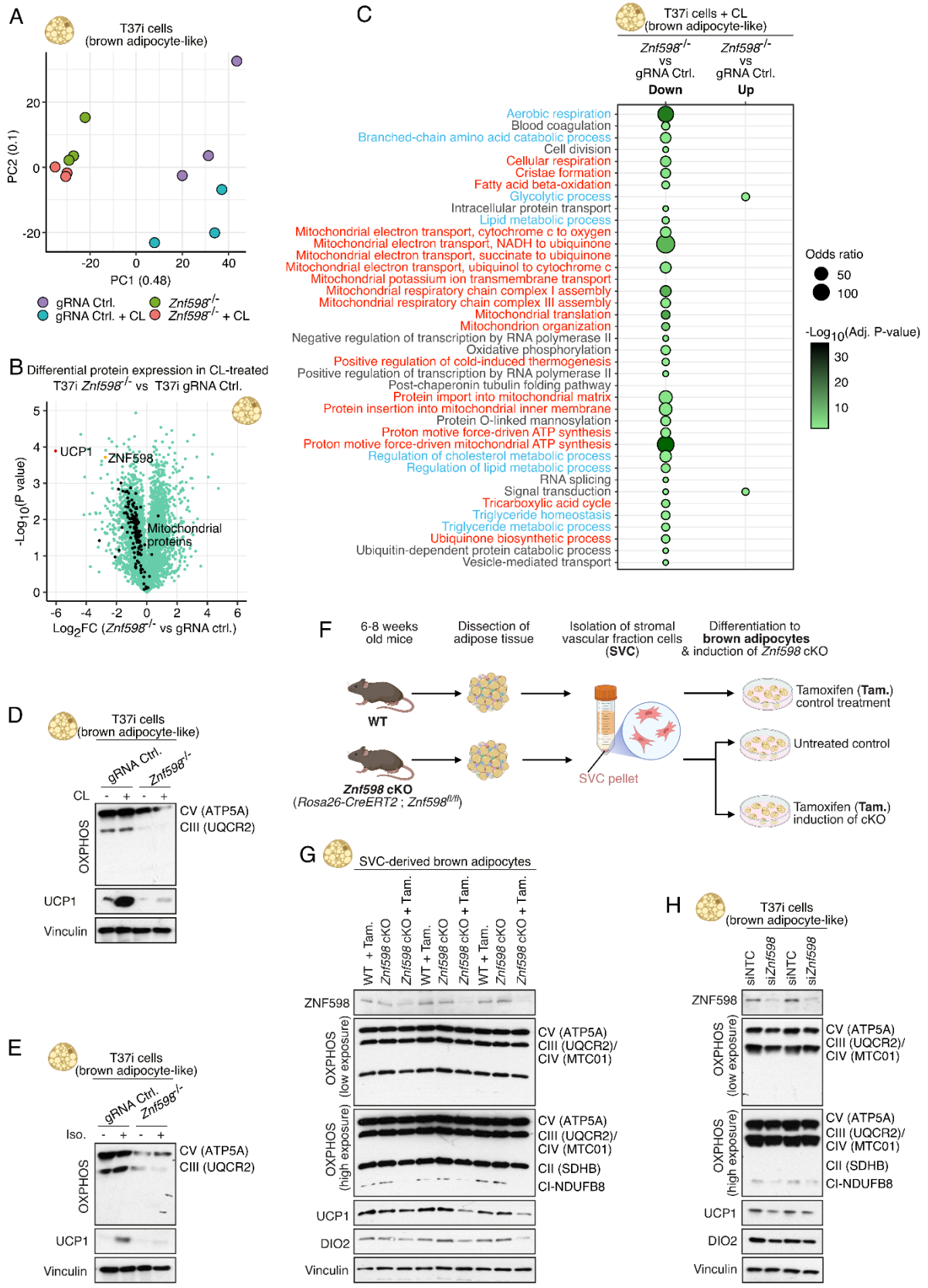
A
T37i cells
(brown adipocyte-like)
PC2 (0.1)
PC1 (0.48)
gRNA Ctrl.
gRNA Ctrl. + CL
Znf598-/-
Znf598-/- + CL
B Differential protein expression in CL-treated
T37i Znf598-/- vs T37i gRNA Ctrl.
UCP1
ZNF598
Mitochondrial proteins
-Log10(P value)
Log2FC (Znf598-/- vs gRNA ctrl.)
C
T37i cells + CL
(brown adipocyte-like)
Znf598-/- vs gRNA Ctrl.
Down
Znf598-/- vs gRNA Ctrl.
Up
Aerobic respiration
Blood coagulation
Branched-chain amino acid catabolic process
Cell division
Cellular respiration
Cristae formation
Fatty acid beta-oxidation
Glycolytic process
Intracellular protein transport
Lipid metabolic process
Mitochondrial electron transport, cytochrome c to oxygen
Mitochondrial electron transport, NADH to ubiquinone
Mitochondrial electron transport, succinate to ubiquinone
Mitochondrial electron transport, ubiquinol to cytochrome c
Mitochondrial potassium ion transmembrane transport
Mitochondrial respiratory chain complex I assembly
Mitochondrial respiratory chain complex III assembly
Mitochondrial translation
Mitochondrion organization
Negative regulation of transcription by RNA polymerase II
Oxidative phosphorylation
Positive regulation of cold-induced thermogenesis
Positive regulation of transcription by RNA polymerase II
Post-chaperonin tubulin folding pathway
Protein import into mitochondrial matrix
Protein insertion into mitochondrial inner membrane
Protein O-linked mannosylation
Proton motive force-driven ATP synthesis
Proton motive force-driven mitochondrial ATP synthesis
Regulation of cholesterol metabolic process
Regulation of lipid metabolic process
RNA splicing
Signal transduction
Tricarboxylic acid cycle
Triglyceride homeostasis
Triglyceride metabolic process
Ubiquinone biosynthetic process
Ubiquitin-dependent protein catabolic process
Vesicle-mediated transport
Odds ratio
50
100
-Log10(Adj. P-value)
30
20
10
D
T37i cells
(brown adipocyte-like)
gRNA Ctrl.
Znf598-/-
CL
OXPHOS
CV (ATP5A)
CIII (UQCR2)
UCP1
Vinculin
E
T37i cells
(brown adipocyte-like)
gRNA Ctrl.
Znf598-/-
Iso.
OXPHOS
CV (ATP5A)
CIII (UQCR2)
UCP1
Vinculin
F
6-8 weeks old mice
Dissection of adipose tissue
Isolation of stromal vascular fraction cells (SVC)
Differentiation to brown adipocytes & induction of Znf598 cKO
WT
Znf598 cKO
(Rosa26-CreERT2 ; Znf598fl/fl)
SVC pellet
Tamoxifen (Tam.) control treatment
Untreated control
Tamoxifen (Tam.) induction of cKO
G
SVC-derived brown adipocytes
WT + Tam.
Znf598 cKO
Znf598 cKO + Tam.
ZNF598
OXPHOS (low exposure)
OXPHOS (high exposure)
CV (ATP5A)
CIII (UQCR2)/
CIV (MTC01)
CII (SDHB)
CI-NDUFB8
UCP1
DIO2
Vinculin
H
T37i cells
(brown adipocyte-like)
siNTC
siZnf598
ZNF598
OXPHOS (low exposure)
OXPHOS (high exposure)
CV (ATP5A)
CIII (UQCR2)/
CIV (MTC01)
CII (SDHB)
CI-NDUFB8
UCP1
DIO2
Vinculin

FIGURE 2. ZNF598 is essential for thermogenic programming and mitochondrial biogenesis in adipocytes

(A) Principal component analysis (PCA) of whole proteome quantification datasets from differentiated WT (gRNA Ctrl.) and *Znf598*$^{-/-}$ T37i cells treated with or without β-agonist CL-316,243 (CL) treatment for 8 hours (n = 3 biological replicates).

(B) Volcano plot comparing levels of individual proteins in WT and *Znf598*$^{-/-}$ T37i brown adipocytes treated with CL (8 hours). ZNF598 (orange), UCP1 (red), and mitochondrial proteins (black) are highlighted.

(C) Kyoto Encyclopedia of Genes and Genomes (KEGG) enrichment analysis of pathway differences based on whole proteome data from (B). Mitochondria-associated processes (red) and metabolic processes (blue) are highlighted.

(D–E) Western blot (WB) analysis of protein lysates from WT and *Znf598*$^{-/-}$ T37i brown adipocytes treated with CL **(D)** or isoproterenol (Iso.) **(E)** for 24 hours, using antibodies against OXPHOS, UCP1, and Vinculin.

(F) Isolation of stromal vascular cells (SVC) and *ex vivo* generation of primary brown adipocytes deleted for *Znf598*.

(G–H) WB analysis of protein lysates from **(G)** brown adipocytes derived from stromal vascular cells (SVC) isolated from WT and *Znf598* cKO mice (± Tamoxifen (Tam.) induction) and **(H)** T37i brown adipocytes depleted of ZNF598 by siRNA (si*Znf598*), using the indicated antibodies.

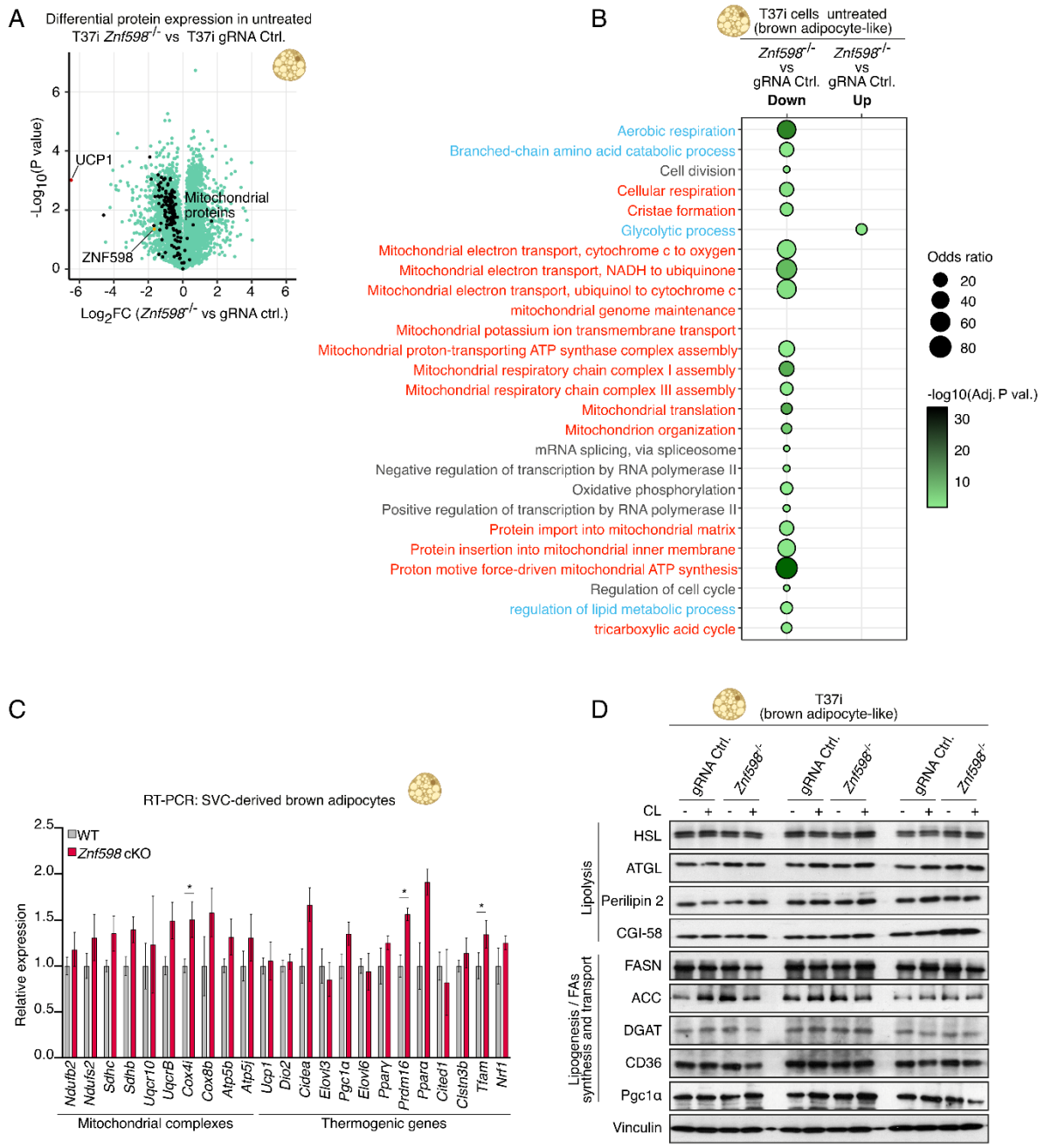

FIGURE S2. Reduced levels of mitochondrial and thermogenic proteins in ZNF598-deficient adipocytes

(A) Volcano plot comparing levels of individual proteins in mock-treated WT (gRNA Ctrl.) and *Znf598*$^{-/-}$ T37i brown adipocytes. ZNF598 (orange), UCP1 (red), and mitochondrial proteins (black) are highlighted.

(B) Kyoto Encyclopedia of Genes and Genomes (KEGG) enrichment analysis of pathway differences based on whole proteome data from (A). Mitochondria-associated processes (red) and metabolic processes (blue) are highlighted.

(C) RT-PCR analysis for expression of mitochondrial and thermogenic genes in brown adipocytes derived from stromal vascular cells (SVC) isolated from WT and *Znf598* cKO mice (+ Tamoxifen induction). Relative expression values (Ctrl. = 1) are plotted as mean, and all error bars represent the SEM (n = 4 biological replicates). *, $p \leq 0.05$ in Mann-Whitney test.

(D) Western blot (WB) analysis of protein lysates from WT and *Znf598*$^{-/-}$ T37i brown adipocytes treated with CL-316,243 (CL) for 24 hours, using the indicated antibodies.

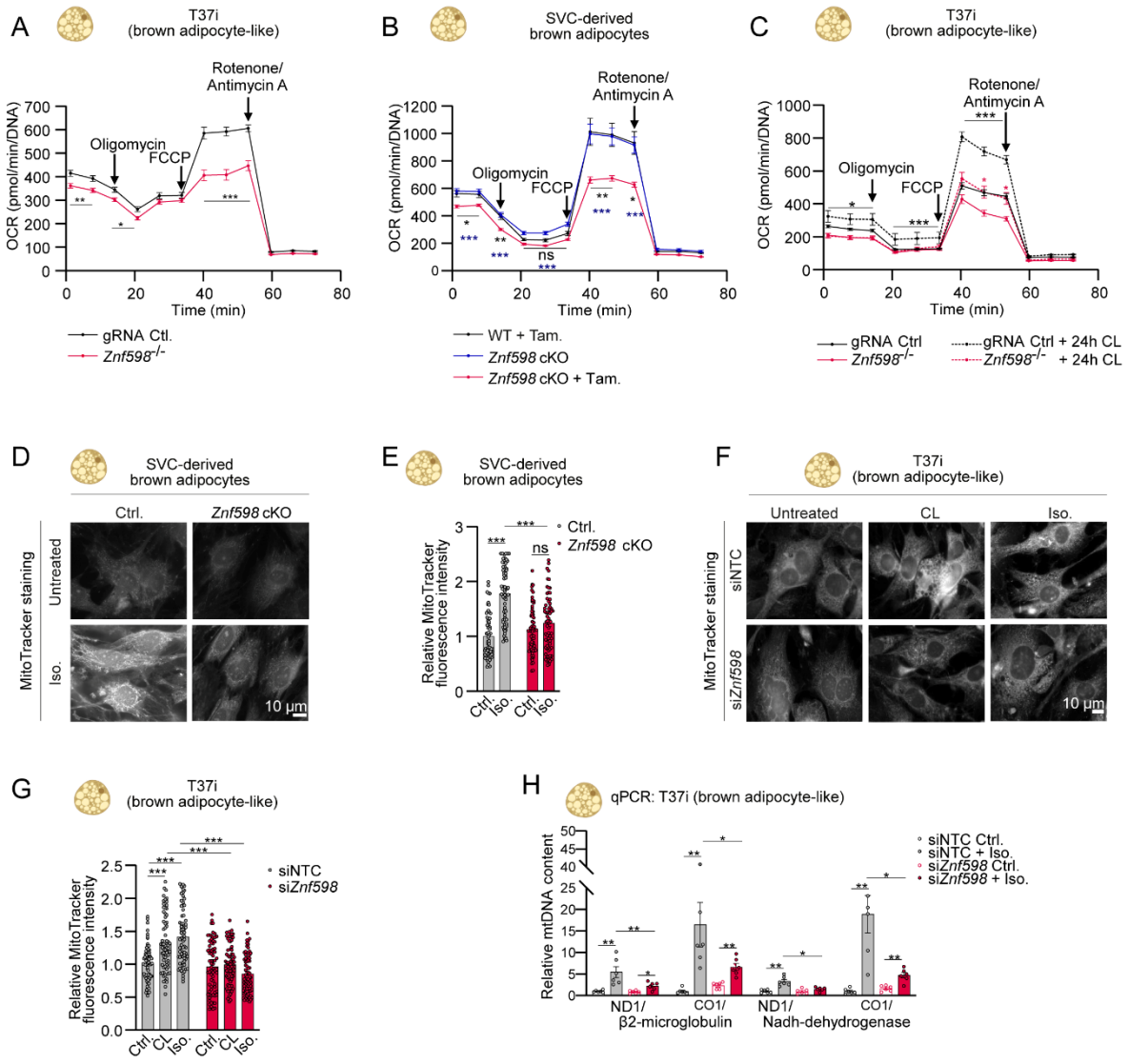

FIGURE 3. ZNF598 is required for β-adrenergic–stimulated mitochondrial respiration.

(A-C) Seahorse analysis of mitochondrial respiration in **(A)** mock-treated WT (gRNA Ctrl.) and *Znf598*$^{-/-}$ T37i brown adipocytes, **(B)** brown adipocytes from stromal vascular cells (SVC) isolated from WT and *Znf598* cKO mice (± Tamoxifen (Tam.) induction), and **(C)** WT and *Znf598*$^{-/-}$ T37i brown adipocytes non-treated (NT) or treated with CL-316,243 (CL) for 24 hours.

(D–E) Staining **(D)** and quantification of mitochondrial content by mitotracker fluorescence **(E)** in brown adipocytes derived from SVC isolated from WT and *Znf598* cKO mice (+

Tamoxifen induction) and treated with isoproterenol (Iso.) for 24 hours. Each data point represents the relative fluorescence intensity of an image field containing 10–15 cells.

(F–G) As in (D) and (E), except that T37i-derived brown adipocytes were transfected with the indicated siRNAs (NTC, non-targeting control) and treated with CL and Iso. for 24 hours.

(H) Quantitative PCR analysis of mitochondrial (mt)DNA levels relative to genomic DNA levels in T37i brown adipocytes depleted of ZNF598 by siRNA and treated with Iso. for 24 hours. Four independent primer sets targeting mtDNA were used.

(A, B, C) All data points are an average of 11-19 replicates and (H) n = 6, corresponding to a technical duplicate of 3 biological replicates each. Data are plotted as mean, and all error bars represent the SEM. ns., non-significant; *, $p \leq 0.05$; **, $p \leq 0.01$; ***, $p \leq 0.001$ in Mann-Whitney test.

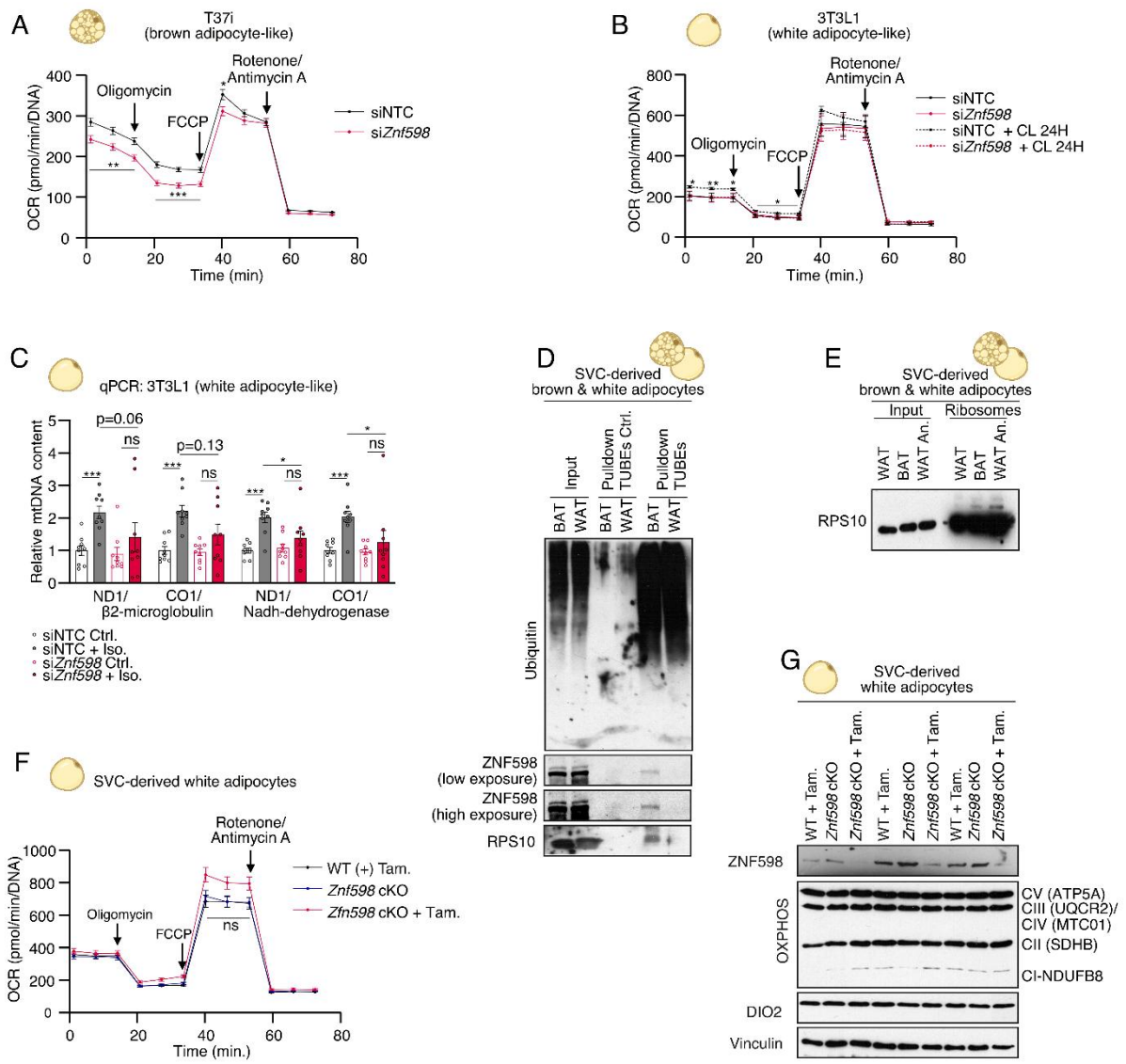

FIGURE S3. β-adrenergic stimulation marginally promotes ZNF598-dependent respiration in white adipocytes.

(A-B) Seahorse analysis of mitochondrial respiration in **(A)** T37i brown adipocytes depleted of ZNF598 by siRNA (si*Znf598*) or transfected with non-targeting control (NTC) and **(B)** 3T3L1 white adipocytes depleted of ZNF598 by siRNA (si*Znf598*) or transfected with non-targeting control (NTC), either non-treated (NT) or treated with CL-316,243 (CL) for 24 hours.

(C) Quantitative PCR analysis of mitochondrial (mt)DNA levels relative to genomic DNA levels in 3T3L1-derived white adipocytes depleted of ZNF598 by siRNA and treated with Iso. for 24 hours. Four independent primer sets targeting mtDNA were used.

(D) Enrichment of ubiquitinated proteins by Agarose-TUBE2 pulldown from brown (BAT) and white (WAT) adipocytes derived from mouse stromal vascular cells (SVC). Western blot (WB) analysis of protein lysates (input) and pulldowns using antibodies against Ubiquitin, ZNF598, and RPS10.

(E) WB analysis of protein lysates (input) and pelleted ribosomes from WAT and BAT from (D). WAT cells were treated with anisomycin (An., 1 hour) as a positive control.

(F) Seahorse analysis of cellular respiration and **(G)** WB analysis of protein lysates from white adipocytes derived from SVC isolated from WT and *Znf598* cKO mice (± Tamoxifen (Tam.) induction).

(A, B, F) All data points are an average of 12-22 replicates and (C) n = 9, corresponding to technical triplicates of 3 biological replicates. Data are plotted as mean, and all error bars represent the SEM. ns., non-significant; *, $p \leq 0.05$; ***, $p \leq 0.001$ in Mann-Whitney test.

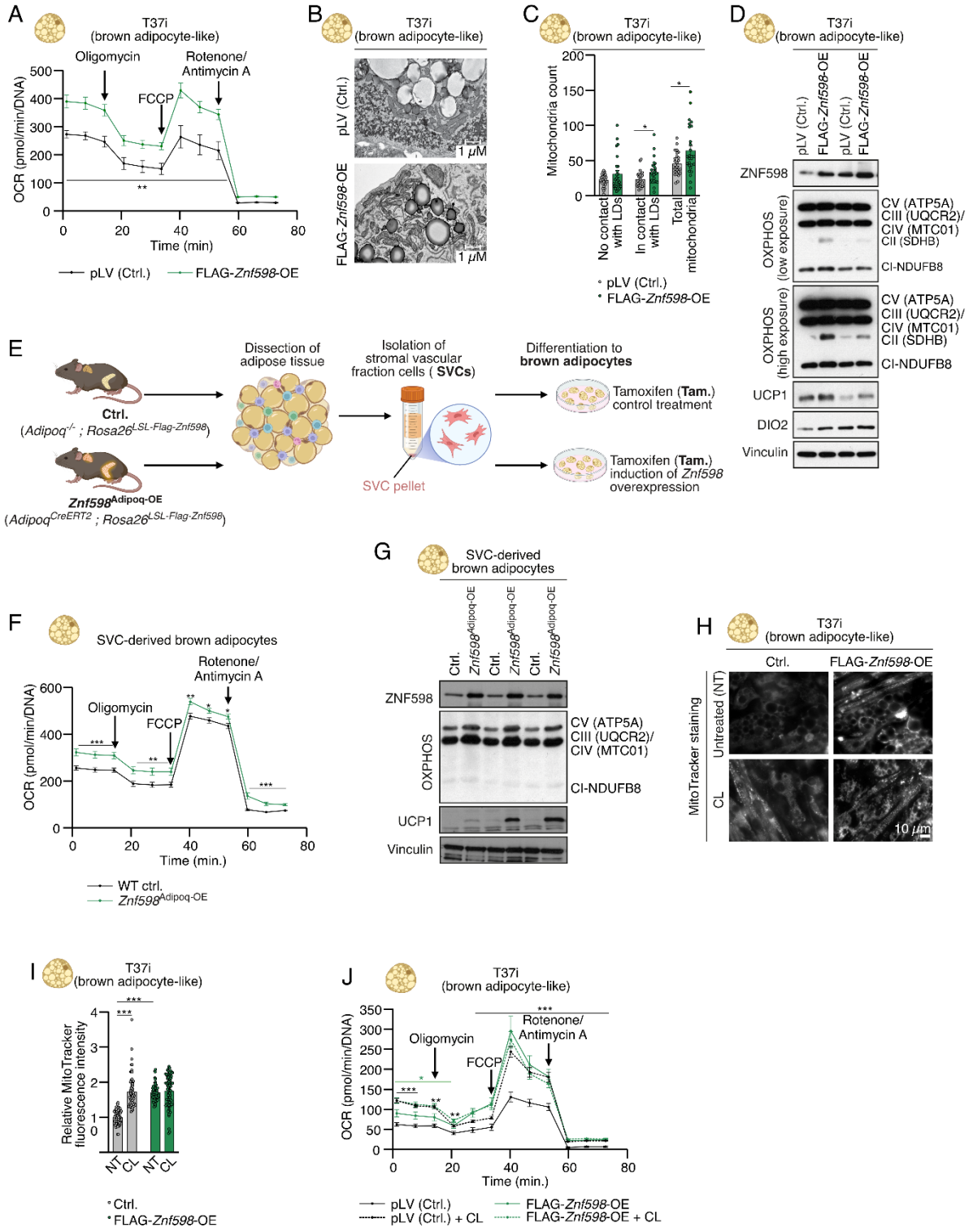

FIGURE 4. Overexpression of ZNF598 elevates respiration and mitochondrial content.

(A) Seahorse analysis of mitochondrial respiration in T37i brown adipocytes stably transfected with empty vector (pLV) or overexpressing ZNF598.

(B-C) Representative electron microscopy images **(B)** and quantification of the number of mitochondria per cell **(C)** of cells from (A). LD, Lipid droplets.

(D) Western blot (WB) analysis of protein lysates from cells from (A), using antibodies against OXPHOS, UCP1, DIO2, and Vinculin.

(E) *Ex vivo* generation of primary brown adipocytes conditionally overexpressing FLAG-ZNF598. Stromal vascular cells (SVC) were isolated from white adipose tissue (WAT) from mice with the indicated genotypes, treated with tamoxifen, and differentiated *in vitro* into brown adipocytes.

(F) Seahorse analysis of mitochondrial respiration in brown adipocytes derived from SVC isolated from control mice and mice with tamoxifen-inducible overexpression of ZNF598 in adipocytes (*Znf598*$^{\text{Adipoq-OE}}$).

(G) Western blot (WB) analysis of protein lysates from cells from (E) and (F), using the indicated antibodies.

(H–I) Staining **(H)** and quantification of mitochondrial content by mitotracker fluorescence **(I)** in cells from (A) non-treated (NT) or treated with CL-316,243 (CL) for 24 hours. Each data point represents the relative fluorescence intensity of an image field containing 10–15 cells.

(J) Seahorse analysis of mitochondrial respiration in cells from (A) non-treated (NT) or treated with CL for 24 hours.

(A, F, J) All data points are an average of more than 7 replicates. Data are plotted as mean, and all error bars represent the SEM. ns., non-significant; *, $p \leq 0.05$; **, $p \leq 0.01$; ***, $p \leq 0.001$ in Mann-Whitney test.

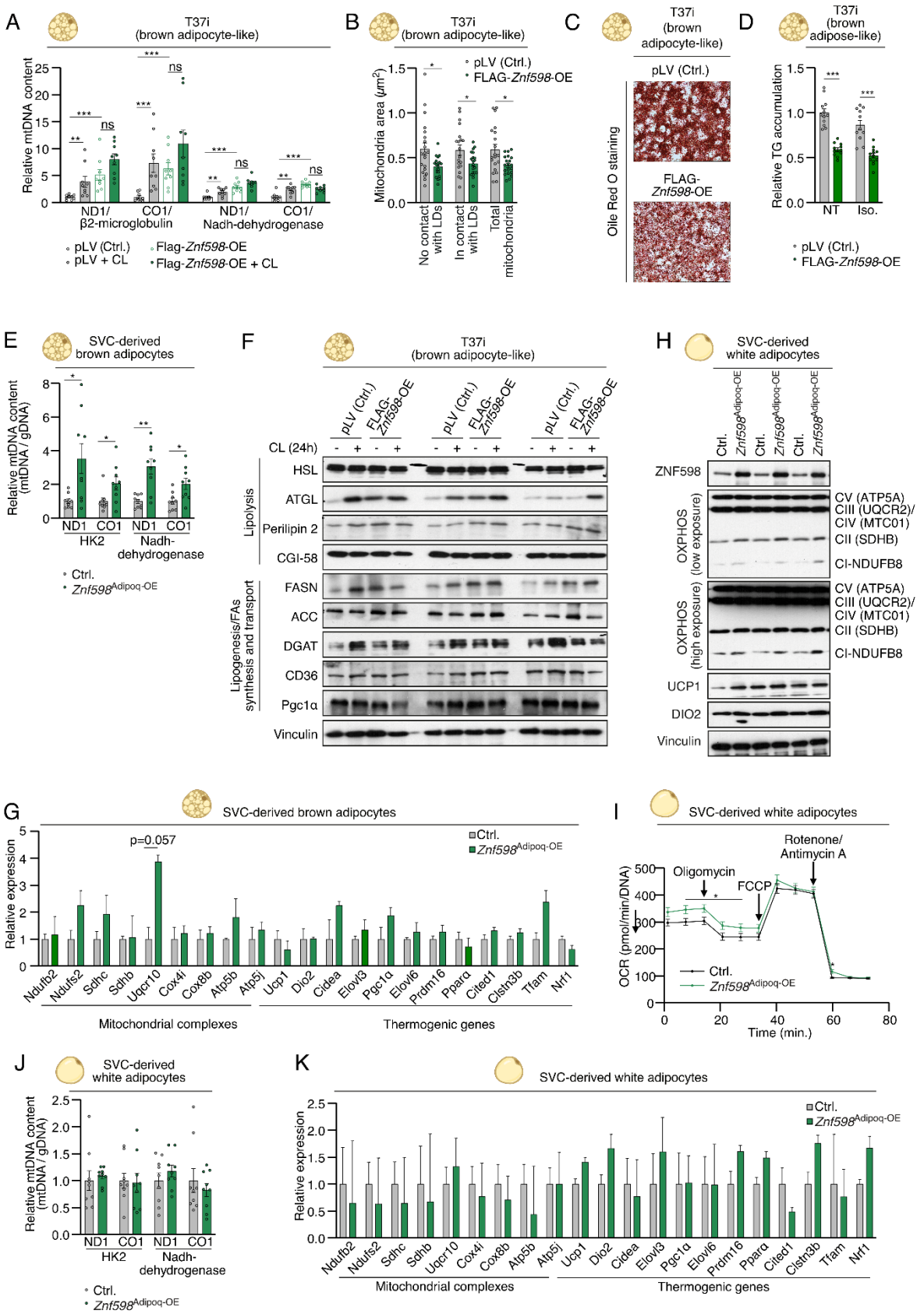
A
T37i
(brown adipocyte-like)
Relative mtDNA content
ND1/
β2-microglobulin
CO1/
ND1/
Nadh-dehydrogenase
CO1/
pLV (Ctrl.)
pLV + CL
Flag-Znf598-OE
Flag-Znf598-OE + CL
B
T37i
(brown adipocyte-like)
Mitochondria area (μm²)
pLV (Ctrl.)
FLAG-Znf598-OE
No contact with LDs
In contact with LDs
Total mitochondria
C
T37i
(brown adipocyte-like)
pLV (Ctrl.)
FLAG-Znf598-OE
Oile Red O staining
D
T37i
(brown adipose-like)
Relative TG accumulation
NT
Iso.
pLV (Ctrl.)
FLAG-Znf598-OE
E
SVC-derived
brown adipocytes
Relative mtDNA content (mtDNA / gDNA)
ND1
CO1
HK2
Nadh-dehydrogenase
Ctrl.
Znf598Adipoq-OE
F
T37i
(brown adipocyte-like)
pLV (Ctrl.)
FLAG-Znf598-OE
CL (24h)
Lipolysis
HSL
ATGL
Perilipin 2
CGI-58
Lipogenesis/FAs synthesis and transport
FASN
ACC
DGAT
CD36
Pgc1α
Vinculin
H
SVC-derived
white adipocytes
Ctrl.
Znf598Adipoq-OE
ZNF598
OXPHOS (low exposure)
OXPHOS (high exposure)
CV (ATP5A)
CIII (UQCR2)/
CIV (MTC01)
CII (SDHB)
CI-NDUFB8
UCP1
DIO2
Vinculin
G
SVC-derived brown adipocytes
Relative expression
p=0.057
Ctrl.
Znf598Adipoq-OE
Ndufb2
Ndufs2
Sdhc
Sdhb
Uqcr10
Cox4i
Cox8b
Atp5b
Atp5j
Ucp1
Dio2
Cidea
Elovl3
Pgc1α
Elovl6
Prdm16
Pparα
Cited1
Clstn3b
Tfam
Nrf1
Mitochondrial complexes
Thermogenic genes
I
SVC-derived white adipocytes
Rotenone/
Antimycin A
Oligomycin
FCCP
OCR (pmol/min/DNA)
Ctrl.
Znf598Adipoq-OE
Time (min.)
J
SVC-derived
white adipocytes
Relative mtDNA content (mtDNA / gDNA)
ND1
CO1
HK2
Nadh-dehydrogenase
Ctrl.
Znf598Adipoq-OE
K
SVC-derived white adipocytes
Relative expression
Ctrl.
Znf598Adipoq-OE
Mitochondrial complexes
Thermogenic genes

FIGURE S4. Effects of ZNF598 overexpression on levels of thermogenic and mitochondrial proteins.

(A) Quantitative PCR analysis of mitochondrial (mt)DNA levels relative to genomic DNA levels in T37i brown adipocytes stably transfected with empty vector (pLV) or overexpressing ZNF598. Cells were left non-treated (Ctrl.) or treated with CL-316,243 (CL) for 24 hours. Four independent primer sets targeting mtDNA were used. Data are plotted as relative expression values (Non-treated Ctrl. = 1). **(B)** Quantification of mitochondrial area in electron microscopy images of cells from (A). LD, Lipid droplets.

(C-D) Representative images of staining **(C)** and quantification **(D)** of cells from (A) for triglycerides and other neutral lipids using AdipoRed reagent. Data are plotted as relative values (Non-treated Ctrl. = 1).

(E) As in (A), except for brown adipocytes derived from stromal vascular cells (SVC) isolated from control mice and mice with tamoxifen-inducible overexpression of ZNF598 in adipocytes (*Znf598*$^{\text{Adipoq-OE}}$).

(F) Western blot (WB) analysis of protein lysates from cells from (A). Cells were left non-treated or treated with CL for 24 hours.

(G) RT-PCR analysis for expression of mitochondrial and thermogenic genes in brown adipocytes from (E). Data are plotted as relative expression values (Ctrl. = 1).

(H) Western blot (WB) analysis of protein lysates from white adipocytes derived from SVC isolated from control mice and mice with tamoxifen-inducible overexpression of ZNF598 in adipocytes (*Znf598*$^{\text{Adipoq-OE}}$), using antibodies against ZNF598, OXPHOS, UCP1, DIO2, and Vinculin.

(I) Seahorse analysis of mitochondrial respiration in white adipocytes from (H).

(J) As in (E), using cells from (H).

(K) As in (G), using cells from (H).

(A, E, J) n = 9 corresponding to technical triplicate of 3 biological replicates, (D) n = 11-12 from 3 biological replicates, (G, K) n = 3-4 biological replicates, and (I) all data points are an average of 23 (Ctrl.) or 36 ($Znf598^{Adipoq\text{-}OE}$) replicates. Data are plotted as mean, and all error bars represent the SEM. ns., non-significant; *, $p \leq 0.05$; **, $p \leq 0.01$; ***, $p \leq 0.001$ in Mann-Whitney test.

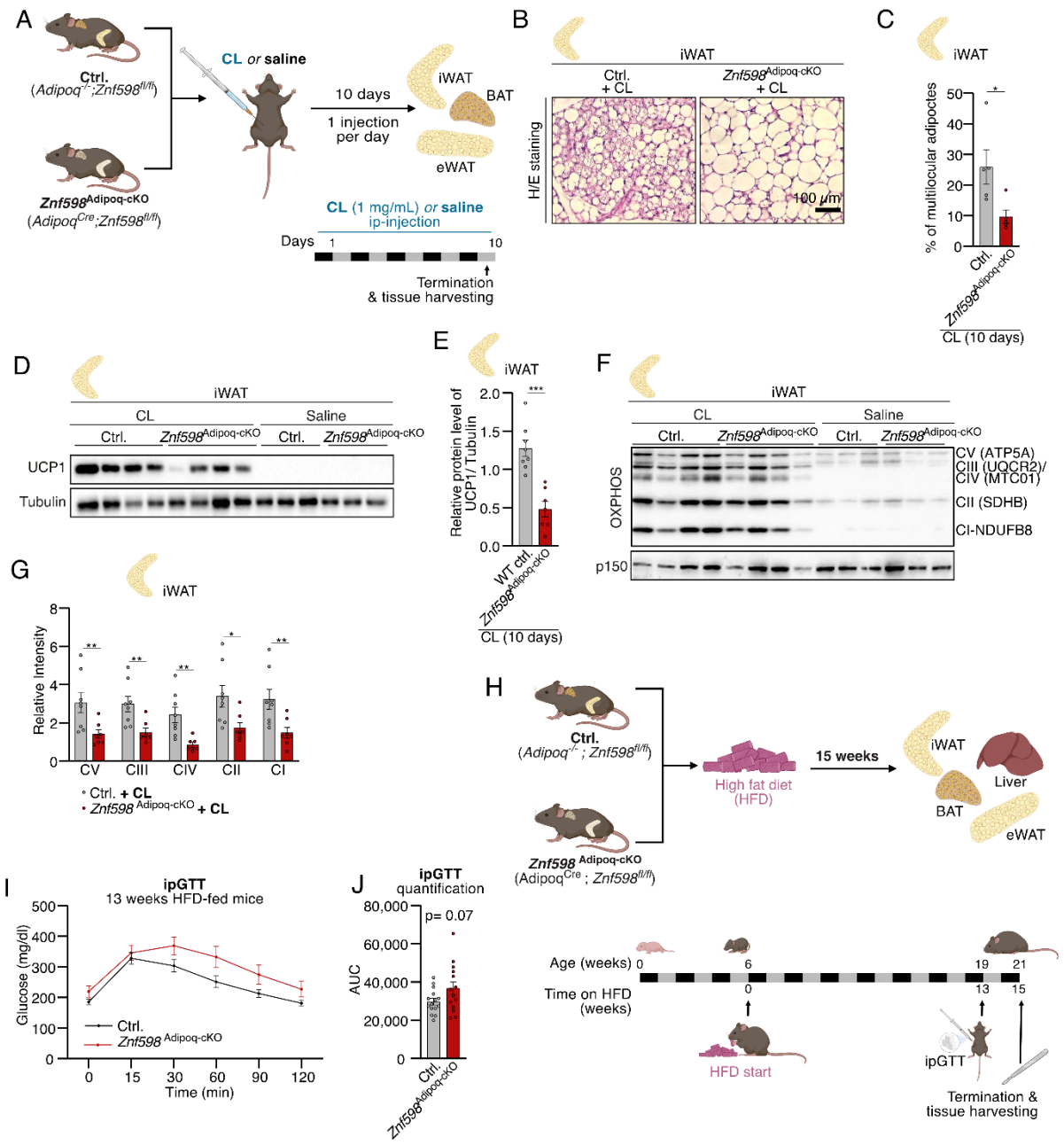

FIGURE 5. Adipocyte-specific deletion of ZNF598 impairs β-adrenergic stimulation-induced iWAT browning and promotes glucose intolerance in mice.

(A) *In vivo* experimental strategy to study thermogenic responses. WT and *Znf598*$^{\text{Adipoq-cKO}}$ (n = 8 and n = 7 biological replicates, respectively) mice were injected with CL-316,243 (CL) for 10 days before euthanasia.

(B) Representative H/E (hematoxylin and eosin) staining of inguinal white adipose tissue (iWAT) in mice from (A).

(C) Percentage of multilocular (brown/beige) adipocytes in iWAT of mice from (A). 5 mice from each group were randomly selected.

(D-E) Western blot (WB) analysis **(D)** and corresponding densitometric quantification **(E)** of UCP1 protein levels in lysates from iWAT of mice from (A).

(F-G) Western blot (WB) analysis **(F)** and corresponding densitometric quantification **(G)** of mitochondrial protein complexes in lysates from iWAT of mice from (A).

(H) Schematic of high-fat diet (HFD)-feeding experiment. Mice with the indicated genotypes were changed from chow to HFD at 6 weeks of age. At 19 weeks of age, mice were challenged by Glucose tolerance test (ipGTT) and euthanized two weeks later.

(I) ipGTT of mice with genotypes from (A) fed a high-fat diet (HFD) as in (H) (n = 15 and n = 14 biological replicates of Ctrl. and *Znf598*$^{\text{Adipoq-cKO}}$, respectively).

(J) Quantification of the area under the curve (AUC) for all mice in (I).

Data are plotted as mean, and all error bars represent the SEM. ns., non-significant; *, $p \leq 0.05$; **, $p \leq 0.01$; ***, $p \leq 0.001$ in Mann-Whitney test.

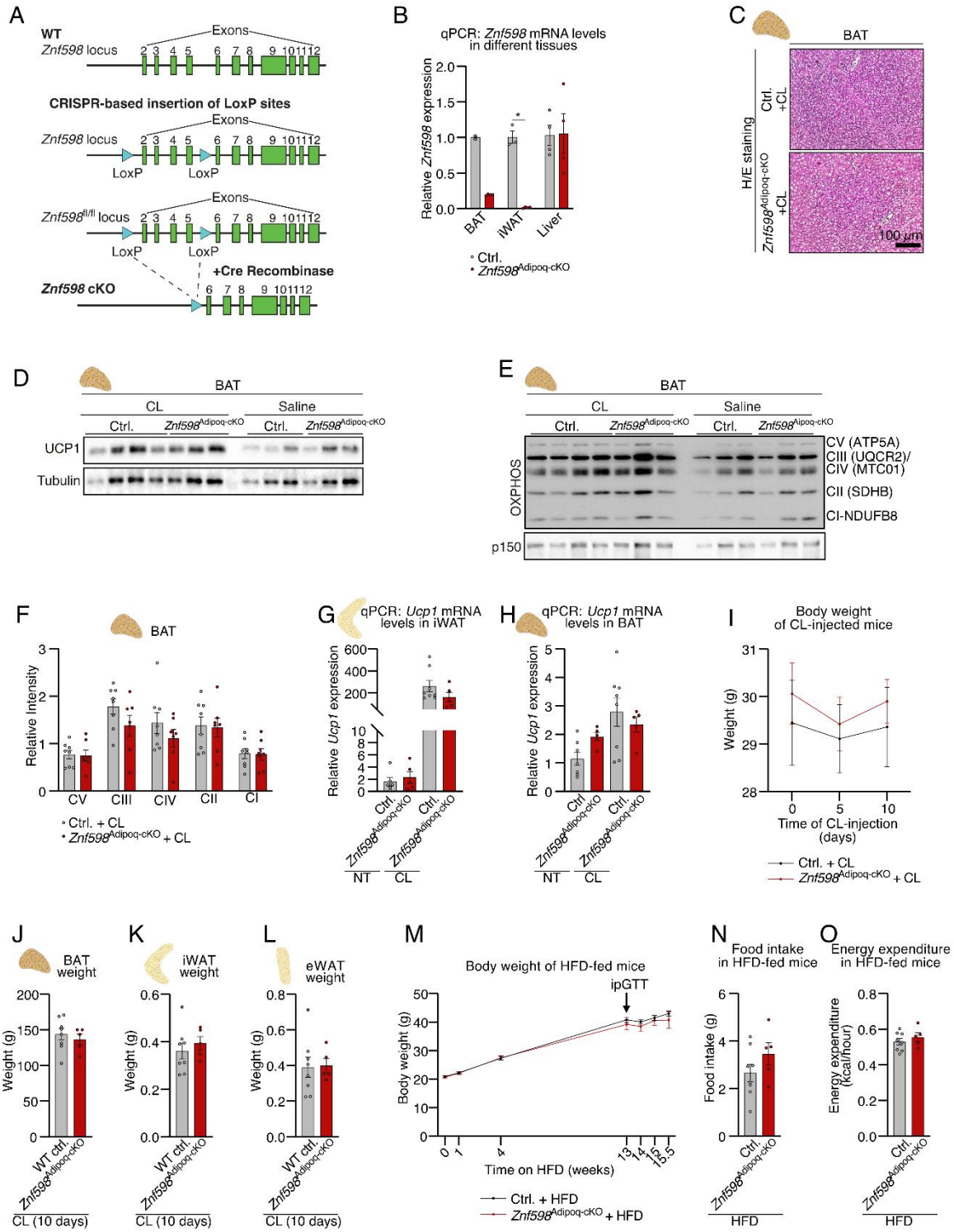

FIGURE S5. CL-316,243 injection does not affect energy balance in *Znf598*$^{\text{Adipoq-cKO}}$ mice.

(A) Schematic of the floxed *Znf598* allele and its targeting by CRE-LoxP in *Znf598*$^{\text{Adipoq-cKO}}$ mice.

(B) qPCR analysis of relative *Znf598* mRNA levels in brown adipose tissue (BAT), inguinal white adipose tissue (iWAT), and liver in WT and *Znf598*$^{\text{Adipoq-KO}}$ mice.

(C) Representative H/E (hematoxylin and eosin) staining of BAT from WT and *Znf598*$^{\text{Adipoq-cKO}}$ mice after injection of CL-316,243 (CL) or saline for 10 days.

(D) Western blot (WB) analysis of UCP1 protein levels in lysates from BAT of mice from (A) treated as in (C).

(E-F) WB analysis **(E)** and corresponding densitometric quantification **(F)** of mitochondrial protein complexes in lysates from BAT of mice from (A) treated as in (C).

(G-H) qPCR analysis of relative *Ucp1* mRNA levels in iWAT **(G)** and BAT **(H)** of mice from (A) treated as in (C).

(I) Changes in body weight of mice from (A) over the course of the CL-injection experiment in (C).

(J-L) BAT **(J)**, iWAT **(K)**, and eWAT (epididymal white adipose tissue) **(L)** weight at day 10 of the CL-injection experiment in (C).

(M-O) Body weight evolution **(M)**, food intake **(N)**, and energy expenditure **(O)** of WT and *Znf598*$^{\text{Adipoq-cKO}}$ mice fed a high-fat diet (HFD) for 15.5 weeks.

(M) n = 15 and n = 14 biological replicates of Ctrl. and *Znf598*$^{\text{Adipoq-cKO,}}$ respectively. (N-O) n = 8 Ctrl. and n = 5 biological replicates of Ctrl. and *Znf598*$^{\text{Adipoq-cKO}}$, respectively, randomly selected from the main experimental group. Data are plotted as mean, and all error bars represent the SEM. ns., non-significant; *, $p \leq 0.05$; **, $p \leq 0.01$; ***, $p \leq 0.001$ in Mann-Whitney test.

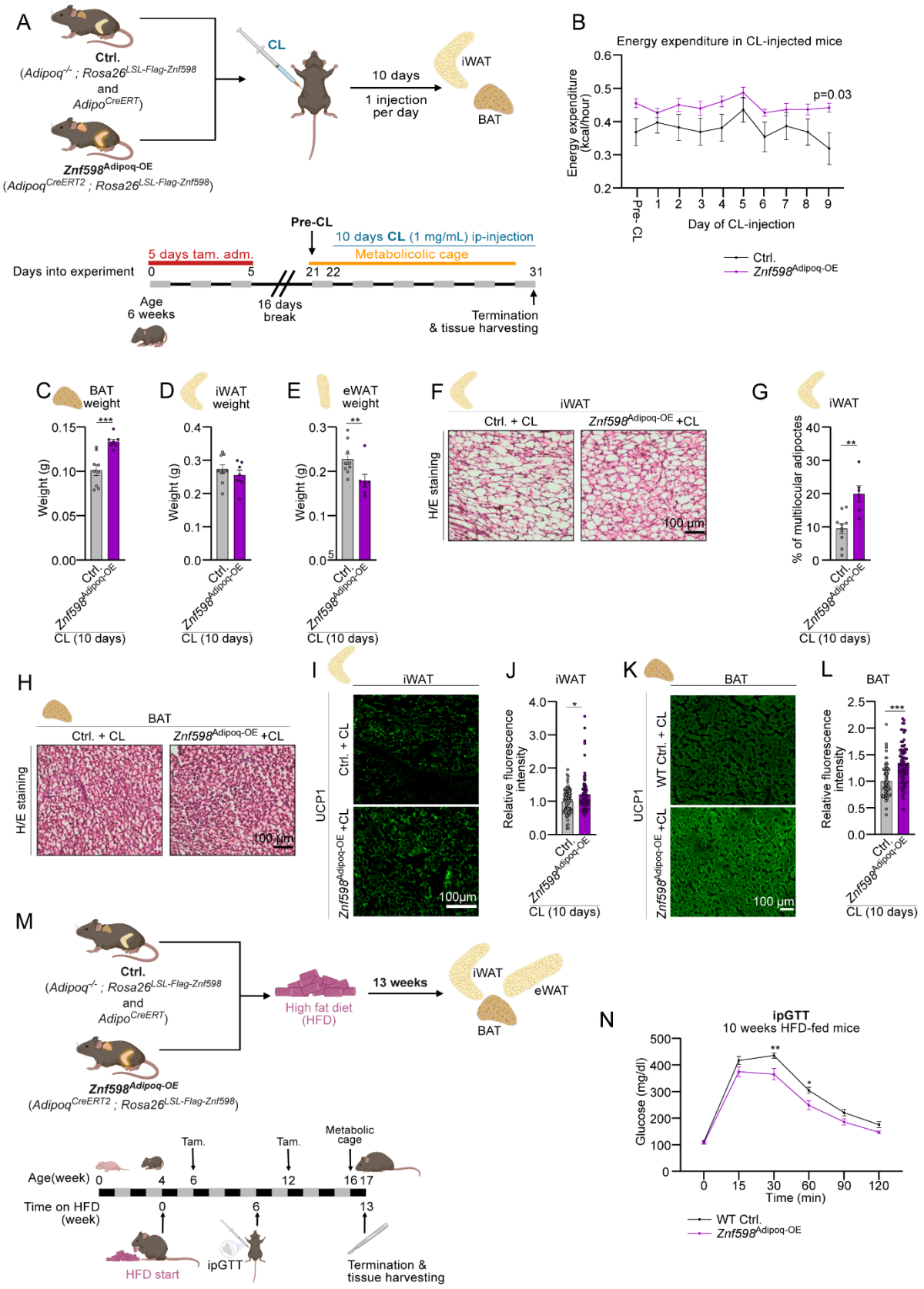
A
Ctrl.
(Adipoq-/- ; Rosa26LSL-Flag-Znf598
and
AdipoCreERT)
Znf598Adipoq-OE
(AdipoqCreERT2 ; Rosa26LSL-Flag-Znf598)
CL
10 days
1 injection
per day
iWAT
BAT
Pre-CL
10 days CL (1 mg/mL) ip-injection
Metabolicolic cage
5 days tam. adm.
Days into experiment
Age
6 weeks
16 days
break
Termination
& tissue harvesting
B
Energy expenditure in CL-injected mice
Energy expenditure (kcal/hour)
p=0.03
Pre-CL
Day of CL-injection
Ctrl.
Znf598Adipoq-OE
C
BAT weight
Weight (g)
CL (10 days)
D
iWAT weight
E
eWAT weight
F
iWAT
Ctrl. + CL
Znf598Adipoq-OE +CL
H/E staining
100 µm
G
iWAT
% of multilocular adipocytes
H
BAT
I
iWAT
UCP1
J
iWAT
Relative fluorescence intensity
K
BAT
WT Ctrl. + CL
L
BAT
M
High fat diet
(HFD)
13 weeks
iWAT
eWAT
BAT
Tam.
Metabolic
cage
Age(week)
Time on HFD
(week)
HFD start
ipGTT
Termination &
tissue harvesting
N
ipGTT
10 weeks HFD-fed mice
Glucose (mg/dl)
Time (min)
WT Ctrl.
Znf598Adipoq-OE

FIGURE 6. Tamoxifen-induced and adipocyte-specific overexpression enhances thermogenesis and protects from glucose intolerance in mice.

(A) *In vivo* experimental strategy to study thermogenic responses in mice overexpressing ZNF598 in adipocytes. WT and *Znf598*$^{\text{Adipoq-OE}}$ (n = 9 and n = 7 biological replicates, respectively) mice were injected with CL-316,243 (CL) for 10 days before euthanasia.

(B) Whole-body energy expenditure of mice from (A) gavaged with tamoxifen or saline and injected as in (A).

(C-E) Brown adipose tissue (BAT) **(C)**, inguinal white adipose tissue (iWAT) **(D)**, and epididymal WAT (eWAT) **(E)** weight at day 10 of the CL-injection experiment in (A).

(F) Representative H/E (hematoxylin and eosin) staining of iWAT of mice from (A)

(G) Percentage of multilocular (brown/beige) adipocytes in iWAT of mice from (A).

(H) Representative H/E (hematoxylin and eosin) staining of BAT of mice from (A)

(I-J) Representative immunostaining images **(I)** and quantification of UCP1 immunofluorescence signal per high-power field **(J)** of iWAT of mice from (A).

(K-L) As in (I-J), except that BAT was immunostained **(K)** and quantified **(L)**.

(M) Schematic of high-fat diet (HFD)-feeding experiment in mice overexpressing ZNF598 in adipocytes. Mice with the indicated genotypes (n = 15 and n = 8 biological replicates of Ctrl. and *Znf598*$^{\text{Adipoq-OE,}}$ respectively) were changed from chow to HFD at 4 weeks of age and gavaged daily with tamoxifen during weeks 4 and 10. At 14 weeks of age, mice were challenged by Glucose tolerance test (ipGTT) and euthanized two weeks later.

(N) ipGTT of mice with genotypes from (A) fed a high-fat diet (HFD) as in (M).

Data are plotted as mean, and all error bars represent the SEM. ns., non-significant; *, p≤0.05; **, p≤0.01; ***, p≤0.001 in Mann-Whitney test.

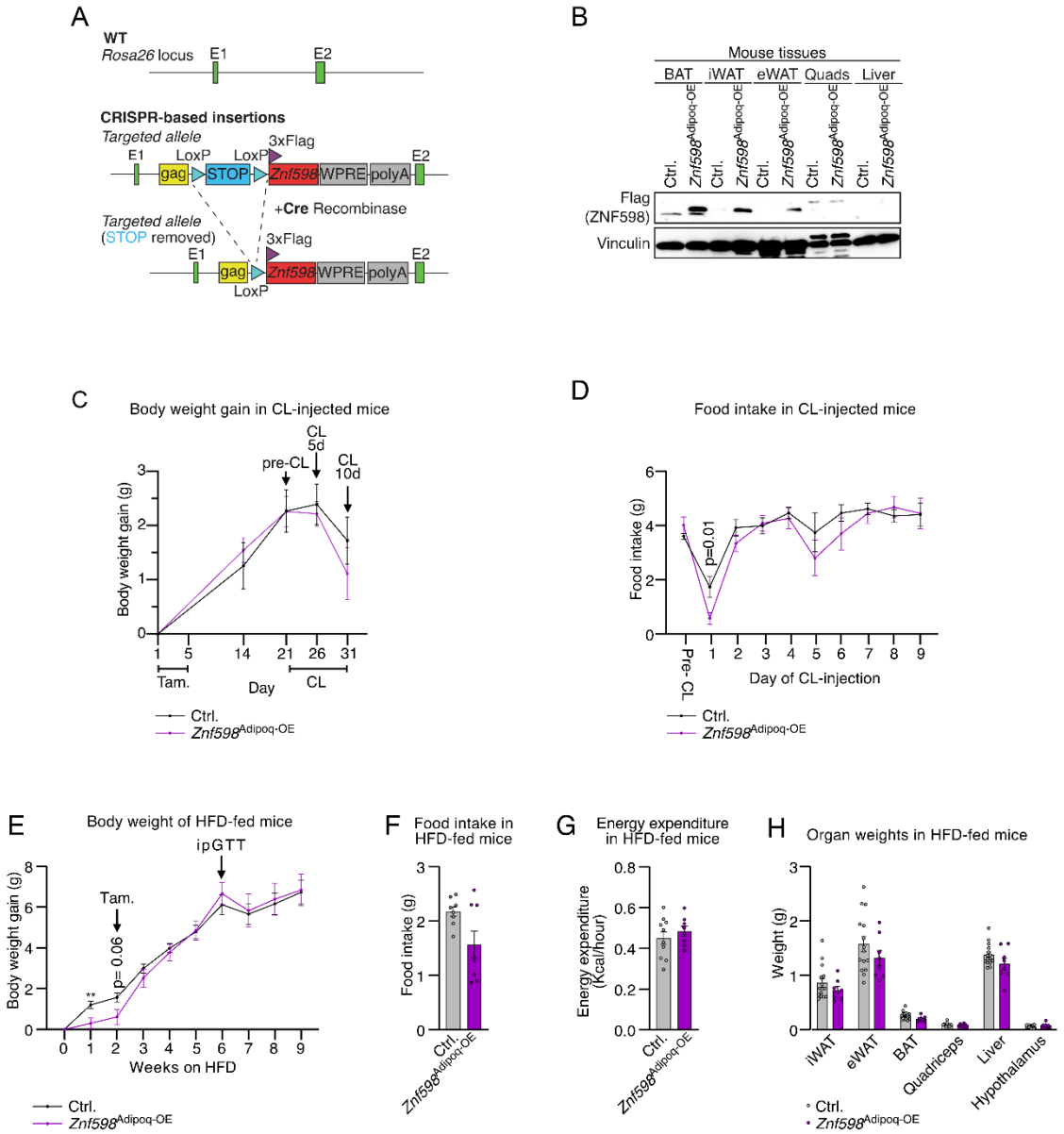

FIGURE S6. Overexpression of ZNF598 in adipose tissue does not affect body composition in HFD-fed mice

(A) Schematic of the Rosa26-integrated *FLAG-Znf598* transgene and its activation by CRE-LoxP upon crossing with AdiponectinCreERT in *Znf598*$^{\text{Adipoq-OE}}$ mice. Recombination and

transgene expression is activated by tamoxifen administration in this model. STOP, stop codon; WPRE, Woodchuck Hepatitis Virus Posttranscriptional Regulatory Element.

(B) Western blot (WB) analysis of FLAG-ZNF598 expression in the indicated adipose tissues, quadriceps muscle (Quad.), and liver in mice from (A) gavaged with tamoxifen or control (Ctrl.) mice.

(C-D) Changes in body weight **(C)** and food intake **(D)** of *Znf598*$^{\text{Adipoq-OE}}$ mice injected with CL-316,243 (CL) (n = 15 and n = 8 biological replicates of Ctrl. and *Znf598*$^{\text{Adipoq-OE}}$, respectively).

(E) Change in bodyweight during the first 9 weeks of high-fat diet (HFD)-feeding of *Znf598*$^{\text{Adipoq-OE}}$ mice.

(F-H) food intake **(F)**, energy expenditure **(G)**, and weight of indicated organs **(H)** at termination of *Znf598*$^{\text{Adipoq-OE}}$ mice fed HFD for 12 weeks (n = 8 biological replicates randomly selected from each experimental group).

Data are plotted as mean, and all error bars represent the SEM. ns., non-significant; *, $p \leq 0.05$; **, $p \leq 0.01$; ***, $p \leq 0.001$ in Mann-Whitney test.

REFERENCES:

Chang, C.-H., Curtis, J.D., Maggi, L.B., Faubert, B., Villarino, A.V., O'Sullivan, D., Huang, S.C.-C., Van Der Windt, G.J., Blagih, J., and Qiu, J. (2013). Posttranscriptional control of T cell effector function by aerobic glycolysis. Cell *153*, 1239-1251.

Chouchani, E.T., Kazak, L., and Spiegelman, B.M. (2019). New advances in adaptive thermogenesis: UCP1 and beyond. Cell metabolism *29*, 27-37.

Chu, J., Hong, N.A., Masuda, C.A., Jenkins, B.V., Nelms, K.A., Goodnow, C.C., Glynne, R.J., Wu, H., Masliah, E., and Joazeiro, C.A. (2009). A mouse forward genetics screen identifies LISTERIN as an E3 ubiquitin ligase involved in neurodegeneration. Proceedings of the National Academy of Sciences *106*, 2097-2103.

Coria, A.R., Shah, A., Shafieinouri, M., Taylor, S.J., Orgebin, E., Guiblet, W., Miller, J.T., Sharma, I.M., and Wu, C.C.-C. (2025). The integrated stress response regulates 18S nonfunctional rRNA decay in mammals. Molecular Cell *85*, 787-801. e788.

D'Orazio, K.N., and Green, R. (2021). Ribosome states signal RNA quality control. Molecular cell *81*, 1372-1383.

De La Cruz, A.C., Tisdale, G., Nakayama, E., Huang, Z., Sinha, N.K., Green, R., and Wu, B. (2025). Single-protein/RNA imaging reveals ZNF598 as a limiting factor in resolving collided ribosomes. The EMBO Journal, 1-18.

Filbeck, S., Cerullo, F., Pfeffer, S., and Joazeiro, C.A. (2022a). Ribosome-associated quality-control mechanisms from bacteria to humans. Molecular cell *82*, 1451-1466.

Filbeck, S., Cerullo, F., Pfeffer, S., and Joazeiro, C.A.P. (2022b). Ribosome-associated quality-control mechanisms from bacteria to humans. Mol Cell *82*, 1451-1466.

Ford, P.W., Garshott, D.M., Narasimhan, M., Ge, X., Jordahl, E.M., Subramanya, S., and Bennett, E.J. (2025). RNF10 and RIOK3 facilitate 40S ribosomal subunit degradation upon 60S biogenesis disruption or amino acid starvation. Cell reports *44*.

Garshott, D.M., An, H., Sundaramoorthy, E., Leonard, M., Vicary, A., Harper, J.W., and Bennett, E.J. (2021). iRQC, a surveillance pathway for 40S ribosomal quality control during mRNA translation initiation. Cell reports *36*.

Garzia, A., Meyer, C., and Tuschl, T. (2021). The E3 ubiquitin ligase RNF10 modifies 40S ribosomal subunits of ribosomes compromised in translation. Cell Reports *36*.

Geng, J., Li, S., Li, Y., Wu, Z., Bhurtel, S., Rimal, S., Khan, D., Ohja, R., Brandman, O., and Lu, B. (2024). Stalled translation by mitochondrial stress upregulates a CNOT4-ZNF598 ribosomal quality control pathway important for tissue homeostasis. Nature communications *15*, 1637.

Huang, Z., Diehl, F.F., Wang, M., Li, Y., Song, A., Chen, F.X., Rosa-Mercado, N.A., Beckmann, R., Green, R., and Cheng, J. (2025). RIOK3 mediates the degradation of 40S ribosomes. Molecular cell *85*, 802-814. e812.

Ikeuchi, K., Izawa, T., and Inada, T. (2018). Recent Progress on the Molecular Mechanism of Quality Controls Induced by Ribosome Stalling. Front Genet *9*, 743.

Inagaki, T., Sakai, J., and Kajimura, S. (2016). Transcriptional and epigenetic control of brown and beige adipose cell fate and function. Nature reviews Molecular cell biology *17*, 480-495.

Juszkiewicz, S., Chandrasekaran, V., Lin, Z., Kraatz, S., Ramakrishnan, V., and Hegde, R.S. (2018). ZNF598 Is a Quality Control Sensor of Collided Ribosomes. Mol Cell *72*, 469-481.e467.

Juszkiewicz, S., and Hegde, R.S. (2017). Initiation of Quality Control during Poly(A) Translation Requires Site-Specific Ribosome Ubiquitination. Mol Cell *65*, 743-750.e744.

Juszkiewicz, S., Speldewinde, S.H., Wan, L., Svejstrup, J.Q., and Hegde, R.S. (2020). The ASC-1 complex disassembles collided ribosomes. Molecular cell *79*, 603-614. e608.

Kim, K.Q., and Zaher, H.S. (2022). Canary in a coal mine: collided ribosomes as sensors of cellular conditions. Trends Biochem Sci *47*, 82-97.

Klingenspor, M., Ivemeyer, M., Wiesinger, H., Haas, K., Heldmaier, G., and Wiesner, R.J. (1996). Biogenesis of thermogenic mitochondria in brown adipose tissue of Djungarian hamsters during cold adaptation. Biochemical Journal *316*, 607-613.

Lehmann, J.A., Lindner, D., Sung, H.-M., and Stoecklin, G. (2024). E3 ubiquitin ligase RNF10 promotes dissociation of stalled ribosomes and responds to ribosomal subunit imbalance. Nature Communications *15*, 10350.
Martin, P.B., Kigoshi-Tansho, Y., Sher, R.B., Ravenscroft, G., Stauffer, J.E., Kumar, R., Yonashiro, R., Müller, T., Griffith, C., and Allen, W. (2020). NEMF mutations that impair ribosome-associated quality control are associated with neuromuscular disease. Nature communications *11*, 4625.
McGirr, T., Onar, O., and Jafarnejad, S.M. (2025). Dysregulated ribosome quality control in human diseases. The FEBS Journal *292*, 936-959.
Monaghan, L., Longman, D., and Cáceres, J.F. (2023). Translation-coupled mRNA quality control mechanisms. The EMBO Journal *42*, e114378.
Narita, M., Denk, T., Matsuo, Y., Sugiyama, T., Kikuguchi, C., Ito, S., Sato, N., Suzuki, T., Hashimoto, S., Machová, I.*, et al.* (2022). A distinct mammalian disome collision interface harbors K63-linked polyubiquitination of uS10 to trigger hRQT-mediated subunit dissociation. Nat Commun *13*, 6411.
Oltion, K., Carelli, J.D., Yang, T., See, S.K., Wang, H.-Y., Kampmann, M., and Taunton, J. (2023). An E3 ligase network engages GCN1 to promote the degradation of translation factors on stalled ribosomes. Cell *186*, 346-362. e317.
Rahmanto, A.S., Blum, C.J., Scalera, C., Heidelberger, J.B., Mesitov, M., Horn-Ghetko, D., Gräf, J.F., Mikicic, I., Hobrecht, R., and Orekhova, A. (2023). K6-linked ubiquitylation marks formaldehyde-induced RNA-protein crosslinks for resolution. Molecular Cell *83*, 4272-4289. e4210.
Rodschinka, G., Forcelloni, S., Kühner, F.M., Wani, S., Riemenschneider, H., Edbauer, D., Behrens, A., and Nedialkova, D.D. (2025). Comparative CRISPRi screens reveal a human stem cell dependence on mRNA translation-coupled quality control. Nature Structural & Molecular Biology *32*, 1932-1946.
Seale, P., Bjork, B., Yang, W., Kajimura, S., Chin, S., Kuang, S., Scime, A., Devarakonda, S., Conroe, H.M., and Erdjument-Bromage, H. (2008). PRDM16 controls a brown fat/skeletal muscle switch. Nature *454*, 961-967.
Silva, J., Alkan, F., Ramalho, S., Snieckute, G., Prekovic, S., Garcia, A.K., Hernández-Pérez, S., van der Kammen, R., Barnum, D., and Hoekman, L. (2022). Ribosome impairment regulates intestinal stem cell identity via ZAKα activation. Nature Communications *13*, 4492.
Sundaramoorthy, E., Leonard, M., Mak, R., Liao, J., Fulzele, A., and Bennett, E.J. (2017). ZNF598 and RACK1 Regulate Mammalian Ribosome-Associated Quality Control Function by Mediating Regulatory 40S Ribosomal Ubiquitylation. Mol Cell *65*, 751-760.e754.
Vind, A.C., Genzor, A.V., and Bekker-Jensen, S. (2020a). Ribosomal stress-surveillance: three pathways is a magic number. Nucleic Acids Res *48*, 10648-10661.
Vind, A.C., Genzor, A.V., and Bekker-Jensen, S. (2020b). Ribosomal stress-surveillance: three pathways is a magic number. Nucleic acids research *48*, 10648-10661.
Zhao, S., Cordes, J., Caban, K.M., Götz, M.J., Mackens-Kiani, T., Veltri, A.J., Sinha, N.K., Weickert, P., Kaya, S., and Hewitt, G. (2023). RNF14-dependent atypical ubiquitylation promotes translation-coupled resolution of RNA-protein crosslinks. Molecular cell *83*, 4290-4303. e4299.

SUPPLEMENTARY MATERIAL

Materials and Methods

Mouse strains and husbandry

To develop a loss-of-function model of ZNF598 in mice, a floxed version of the *Znf598* gene (*Zfp598*; ENSMUSG00000041130) was created by inserting loxP sites upstream of exon 2 and

downstream of exon 5, respectively (Biocytogen). Mice harbouring this floxed allele were crossed with adiponectin-cre mice to establish a C57BL/6 line with deletion of the *Znf598* gene in adipocytes (*Znf598*$^{adipoq\text{-}cKO}$). Mice carrying the floxed allele were also crossed with ROSA26-creERT2 mice (*Znf598* cKO mice), allowing for tamoxifen-induced recombination and gene deletion in all cells and tissues. To develop a gain-of-function model of ZNF598, we generated a transgenic *ROSA26 3xFLAG-Znf598* knock-in (KI) mouse model on a C57BL/6 background by using the EGE® system from Biocytogen Extreme Genome. The coding sequence of 3xFLAG-ZNF598 is preceded by a STOP codon flanked by two loxP sites, resulting in *tgZnf598floxSTOPflox* mice. Therefore, the expression of the transgene will be only possible upon deletion with Cre recombinase. We crossed our mouse model (*tgZnf598floxSTOPflox* mice) with the tamoxifen-inducible adipocytes-specific Cre line (*AdiponectinCreERT*) as previously reported (El-Merahbi et al., 2020) to achieve the *Znf598*$^{adipoq\text{-}OE}$ line. For Cre-ERT2 activation, 100 mg/kg of Tamoxifen (Sigma-Aldrich T5648) was given orally by using a feeding needle for five consecutive days. The efficiency and specificity of overexpression were confirmed by qPCR and Western blotting.

Cell culture

T37i pre-adipocyte cells were cultured in DMEM-F12 with GlutaMAX™ supplement, 10% fetal calf serum (FCS), and 1% Penicillin-Streptomycin (P/S). Differentiation was induced 2 days post-confluence by adding 2 nM T3-hormone and 1.5 µg/ml insulin for 8 to 10 days to achieve differentiation into adipocytes. Fresh agonists were added to the medium every 48 hours. 3T3L1 preadipocytes were cultured in DMEM, high glucose with 10% FCS and 1% P/S. For differentiation, the cells were grown to confluency. Two days after reaching confluency, the medium was switched to DMEM containing 10% fetal bovine serum, 1.5 µg/ml insulin, 0.5 mM 3-isobutyl-1-methylxanthine (IBMX), and 1 µM Dexamethasone (Dex) for 48 hours. This step was repeated for another 48 hours, and then the cells were incubated with

DMEM supplemented with 10% FBS and 1.5 µg/ml insulin for up to 10 days in order to achieve full differentiation. Stromal vascular cells (SVC) from inguinal white adipose tissue (iWAT) and brown adipose tissue (BAT) of 6- to 8-week-old mice were isolated and differentiated into mature adipocytes. iWAT and BAT were sliced and digested in PBS containing 2 mg/mL collagenase D (Sigma-Aldrich), 5 mM CaCl2, and 1% BSA for 30 minutes (min) at 37°C. After digestion, the solution was passed through a 40-µm mesh, centrifuged at 1,000 rpm for 5 min to collect SVCs, and then washed in PBS by centrifugation. SVCs were plated on Matrigel-coated (Corning) plates in DMEM/F-12 with GlutaMAX™ supplement containing 10% FBS, 1% non-essential amino acids (NEAA), and 40 µg/mL gentamycin. Two days post-confluence, SVC differentiation was induced by adding a cocktail including 0.2 µM indomethacin, 1 µM dexamethasone, 0.5 mM IBMX, 0.5 µM Rosiglitazone, and 1.5 µg/ml insulin for the first 4 days, followed by insulin treatment for an additional 4 days to achieve differentiation into adipocytes. In SVC derived from BAT, additionally, 2 nM T3 was added to the medium throughout differentiation. To induce overexpression or knockout of ZNF598 in SVC-derived adipocytes isolated from *Znf598* cKO and *Znf598*$^{adipoq\text{-}OE}$ mice, cells were supplemented with 1 µM tamoxifen on the 3rd day of differentiation for 5 days.

In the indicated experiments, β2-adrenergic agonists, isoproterenol (Tocris Biotech) and CL-316,243 (Tocris Biotech) were supplemented to the differentiation medium at indicated concentrations throughout the differentiation process.) HEK293T cells were maintained in DMEM containing high glucose, 10% FBS, and 1% penicillin–streptomycin.

DNA constructs

The Vectorbuilder lentiviral pLV-CRISPR-Cas9:T2A -U6- Puro system was used to induce long-term gene silencing of the *Znf598* gene in the T37i cell line with the guide sequence CCTGGCTCGACACCGTATGC. Additionally, the mZNF598 and 3xFLAG-mZNF598

overexpressing vectors were also synthesised by Vectorbuilder by the insertion of their respective coding sequences in PLV- EF1A -Puro. EGFP(ns):{P2A}:{FLAG-K(AAA)20}:{P2A}:mKate2 and Mito/EGFP(ns):{P2A}:{FLAG-K(AAA)20}:{P2A}:mKate2 from Vectorbuilder were synthesised by the insertion of their respective coding sequences in PLV-Neo-TRE. Particles were packaged in HEK293T cells with psPAX and pMD2.G. The viral supernatant was collected and filtered (0.45 μm) 48 h later, and T37i cells were infected with the virus and 4 μg/mL polybrene for 48 h. Puromycin (5 μg/mL) or geneticin (1.25 mg/mL) were used for the selection of stable cells.

Proteomics and transcriptomics data comparison – cold challenge

Preprocessed proteomics and transcriptomics data were gathered from the supplementary material in (Sustarsic et al., 2018) and (Bai et al., 2017), choosing the 8h and 6h cold challenge timepoints, respectively. Log2 fold changes were calculated using limma (Ritchie et al., 2015) in R (v4.4.0). We used biomaRt (Durinck et al., 2009) (v2.60.1) to annotate the data, and ggplot2 (Wickham, 2011) (v3.5.1) to visualise it.

RNA-sequencing and data analysis

Cold challenge

Animal studies were performed with approved protocols from The Danish Animal Experiments Inspectorate (permit number: 2018-15-0201-01441) and the University of Copenhagen. 20-week-old C57BL/6NTac (Taconic Biosciences) mice were acclimatised to thermoneutrality (29°C) for 3 weeks, then exposed to 4°C for 24h in a climate chamber (Memmert, HPP750). Termination was performed in the morning, and adipose tissues were snap frozen after collection. Tissues were homogenised using TissueLyser (Qiagen) in 1 mL TRIzol (Invitrogen). Chloroform was added, samples were mixed, subjected to centrifugation, and the aqueous phase

was transferred to a new tube. Thereafter, 1:1 70% ethanol was added, and the total volume was loaded on silica-membrane columns. RNA extraction was performed using a commercially available kit (Rneasy lipid tissue kit, Qiagen) following the manufacturer's protocol. RNA concentration and purity were assessed by absorbance at 260 and 280 nm using NanoDrop One (Thermo Fisher Scientific, Waltham, MA). RNA was checked for quality using the Agilent RNA 600 nano kit and Bioanalyser instrument (Agilent Technologies, Santa Clara, CA). Messenger RNA sequencing was performed by the Single-Cell Omics platform at the Novo Nordisk Foundation Center for Basic Metabolic Research. Libraries were prepared with 250ng RNA using the Universal Plus mRNA-seq with NuQuant protocol (Tecan) as recommended by the manufacturer. Libraries were quantified with NuQuant using the Qubit 2.0 Fluorometer (Thermo Fisher), quality checked using the 4200 TapeStation instrument (Agilent Technologies) and subjected to 101-bp paired-end sequencing on a NovaSeq6000 (Illumina, San Diego, CA, USA).

SVC-derived adipocytes

RNA was isolated from differentiated white or brown adipocytes from SVC of control mice stimulated or not with the β-agonist isoprotenerol in complete medium for 6h using TRIzol reagent (Invitrogen, Waltham, MA, USA) following the manufacturer's instructions. The quality and integrity of total RNA were assessed on an Agilent 2100 Bioanalyzer using the RNA 6000 Nano Kit (Agilent Technologies). Strand-specific, poly(A)-enriched RNA libraries were generated with the KAPA Stranded mRNA Sample Preparation Kit (Kapa Biosystems, MA, USA). Briefly, 500 ng of total RNA was used for mRNA enrichment with poly-T oligo-conjugated magnetic beads (Kapa Biosystems). The purified mRNA was fragmented and converted into first-strand cDNA using reverse transcriptase, followed by second-strand synthesis to obtain double-stranded cDNA (dsDNA). A-tailing and adapter ligation were performed (adapters from NEB, Ipswich, MA, USA), after which the uracil-containing loop

region of the adapters was digested with USER enzyme (NEB). Adapter-ligated fragments were amplified by PCR using NEB primers (Ipswich, MA, USA). Library size and quality were evaluated on the Agilent 2100 Bioanalyzer using the DNA High Sensitivity chip (Agilent Technologies), yielding a mean fragment size of approximately 300 bp. Libraries were quantified with a Quantus fluorometer and the QuantiFluor dsDNA System (Promega, Madison, WI, USA), and subsequently sequenced as 2 × 151 bp paired-end reads on an Illumina NovaSeq 6000 platform (Illumina, San Diego, CA, USA). Initial read quality assessment was carried out using FastQC (v.0.11.9). Adapter trimming and quality filtering were performed with cutadapt (v.3.4) and TrimGalore (v.0.6.7), respectively, with the TrimGalore quality cutoff set to 25. Reads were then aligned to the mouse reference genome (GRCm39) using STAR (v.2.7.9a) with default parameters. Gene annotation was based on the Ensembl release 105 GTF file. Duplicate reads were marked using Picard MarkDuplicates (v.2.27.4-SNAPSHOT). Final quality metrics were compiled with MultiQC (v.1.13), incorporating outputs from RSeQC (v.3.0.1) and the tools listed above. Read summarisation and quantification were conducted with featureCounts (v.2.0.0) using paired-end mode, counting only primary and reversely stranded alignments. A minimum mapping quality threshold of 3 was applied. Differential expression and functional analyses were conducted in R (v.4.1.3). Differential expression analysis was performed with DESeq2 (v.1.34) using default settings; features with fewer than 10 total counts across all samples were excluded. Functional enrichment was assessed using the enrichPathway() function, and gene set enrichment analysis was performed with the gsePathway() function, both from the ReactomePA package (v.1.38). Statistical significance was defined as $p<0.05$. Data visualisation was conducted using ggplot2 (v.3.5.1), enrichplot (v.1.14.1), and ComplexHeatmap (v.2.10.0).

Total proteomics and K-ε-GG enrichment analysis

Proteomics sample preparation

Cells were lysed in EasyPEP lysis buffer (Thermo Fisher Scientific) supplemented with nuclease, followed by mechanical disruption using 1 mL syringes fitted with 26 G needles. Lysates were then heated at 95 °C for 10 minutes. Protein levels were quantified with the Pierce BCA Protein Assay Kit (Thermo), and 500 µg of aliquots were prepared. Proteins were reduced with 5 mM TCEP at 55 °C for 15 minutes and subsequently alkylated with 20 mM CAA for 30 minutes at room temperature (RT). Enzymatic digestion was performed overnight at 37 °C using trypsin and LysC at a 1:50 enzyme-to-protein ratio. Resulting peptides were acidified with 10% formic acid (FA) and purified on a Thermo desalting plate. Peptides were eluted using 150 µL of 40% acetonitrile (ACN) containing 5% ammonium hydroxide, then dried at 45 °C in a SpeedVac concentrator.

K- ε-GG enrichment

Ubiquitylated peptides were enriched using the PTMScan HS Ubiquitin/SUMO Remnant Motif (K-ε-GG) kit (Cell Signaling Technology). Dry peptides were centrifuged at 2000 × g for 5 minutes and resuspended in 750 µL of 1× High-Salt IAP Bind Buffer. The pH was adjusted to ≥7.0 if necessary, using 1 M Tris base. A 40 µL aliquot was taken for global proteome analysis. The remaining peptide solution was clarified by centrifugation at 10,000 × g for 5 minutes at 4 °C and cooled on ice. Antibody beads were prepared by gently mixing the bead slurry, spinning briefly, and washing four times with 1 mL of ice-cold 1× PBS. Soluble peptides were transferred to the beads and incubated on a rotator for 2 hours at 4 °C. After incubation, the tubes were spun down briefly and placed on a magnetic rack. The unbound peptide solution was collected and stored at −20 °C. Beads were then washed four times with 450 µL of chilled 1× HS IAP Wash Buffer and twice with 1 mL of chilled LC-MS grade water. Elution was performed twice by incubating beads with 50 µL of 0.15% TFA for 10 minutes at RT (<800 rpm), followed by magnetic separation. Enriched peptides and global aliquots were desalted using a Thermo desalting plate as described above. Finally, dried peptides were resuspended,

quantified with lunatic and adjusted in MS Buffer A* (0.1% FA, 2% ACN) for downstream MS analysis.

LC–MS Analysis

Peptides were first loaded onto a C18 PepMap trapping column (300 µm ID, Thermo Scientific) using a Vanquish Neo UHPLC system (Thermo Scientific), and subsequently separated on an Aurora Ultimate 25 × 75 µm C18 analytical column (IonOpticks). Chromatographic separation was achieved at 50 °C using a 60-min stepped gradient at a flow rate of 400 nL/min: 2–17% solvent B (0.1% formic acid in acetonitrile) over 33 min, 17–25% B over 11 min, and 25–35% B over 6 min. Eluting peptides were introduced into a Tribrid Ascend mass spectrometer (Thermo Scientific) with a spray voltage of 2200 V. Data were collected in data-independent acquisition (DIA) mode. Full MS scans were acquired in the Orbitrap at 60,000 resolution across 450–1150 m/z, with an AGC target of 250% and a maximum injection time of 123 ms. DIA consisted of 55 windows (12 Th width, 1 Th overlap) spanning 472–1143 m/z, recorded at 15,000 resolution with an AGC target of 1000% and a maximum injection time of 27 ms. Fragmentation was performed using CID with a normalised collision energy (NCE) of 30%.

Data analysis

All statistical analyses were carried out using custom Python scripts (Proteomelit, version 1.1.0), based on the automated analysis pipeline of the Clinical Knowledge Graph (Santos et al., 2022). For post-translational modification (PTM) data, precursors were aggregated into modified peptides by grouping unique modified peptide sequences within each sample and summing their precursor intensities. Intensity values were log2-transformed, and features with fewer than 70% valid values in at least one group were excluded. For the PTM dataset, all statistical and enrichment analyses were conducted exclusively on PTM-modified peptides. Missing values were imputed using a mixed approach: kNN imputation was applied to values missing at random (MAR), and MinProb imputation (width = 0.2, shift = 1.8) was applied to

values missing not at random (MNAR) [Lazar et al., 2016]. MAR was defined as having at least 60% of existing values within a given group. Following imputation, modified peptide intensities were normalised to the corresponding protein abundance in the non-enriched global proteome. Differential expression analysis was performed using unpaired t-tests. Resulting p-values were adjusted for multiple hypothesis testing using a permutation-based False Discovery Rate (FDR) approach. The parameters used were: FDR threshold = 0.01, fold-change (FC) = 1, s0 = 1, and 250 permutations. Functional enrichment analysis for significant features was performed using Fisher's exact test followed by Benjamini–Hochberg correction. Gene Ontology annotations served as the basis for enrichment testing. Analyses were conducted at the protein level for both the global proteome and ubiquitylome datasets. Up-regulated and down-regulated features were treated as the foreground, while all remaining proteins in the dataset constituted the background. Enrichment bubble plots display only terms that are significantly enriched (adjusted p-value) and associated with at least two foreground proteins.

Data availability

The mass spectrometry proteomics data have been deposited to the ProteomeXchange Consortium (http://proteomecentral.proteomexchange.org) via the PRIDE partner repository with the data set identifier PXD069445 for the global proteome and with the data set identifier PXD069447 for the ubiquitylation proteome. (https://www.ebi.ac.uk/pride/archive/projects/)

siRNA transfection

Differentiated adipocytes were detached using Accutase solution for 15 min, spun down at 1,200 rpm for 5 min and counted. The cells were resuspended in culture medium and added to Matrigel-coated culture plates or 96-well Seahorse plates. The indicated siRNAs and Dharmafect-Duo transfection reagent (Dharmacon) were diluted separately in Opti-MEM reduced serum medium before being mixed by pipetting and incubated for 20 min at RT. The

preincubated siRNA-Duofect mix was added on top of the cells. The final concentrations of Duofect, siRNA, and cell number were adjusted per surface area in a ratio of 2.1 µl/cm² Duofect, 1.25 nM/cm² siRNA, and 16.4 × 10^4/cm² cells, respectively. Experiments were conducted on the cells 48 hours after transfection. All siRNA sequences used were ordered as smart pools from Dharmacon.

mKate2/ EGFP ratio calculation

Differentiated adipocytes from EGFP(ns):{P2A}:{FLAG-K(AAA)20}:{P2A}:mKate2 and Mito/EGFP(ns):{P2A}:{FLAG-K(AAA)20}:{P2A}:mKate2 stable cell lines were detached using Accutase solution for 15 min, spun down at 1,200 rpm for 5 min, and counted. The cells were resuspended in culture medium and added to Matrigel-coated ibidi µ-Slide 8 wells. In the indicated experiments, cells were transfected with siRNAs. Control cells and cells treated with β-agonists were imaged using a Zeiss spinning-disk confocal microscope equipped with an HC APO 63×/1.20 water-immersion objective. GFP and mKate fluorescence were excited with 488 nm and 561 nm lasers, respectively, and fluorescence emission was collected using 525/50 nm and 600/50 nm filters for GFP and mKate, respectively. Images were acquired from at least 10 randomly selected fields of view per sample. The fluorescence was quantified using ImageJ software. To create a mask covering all regions exhibiting green and/or red fluorescence, images were pre-processed by applying background subtraction and median filtering, followed by binarization using Otsu thresholding. Red and green fluorescence intensities were then quantified within the masked regions, and after background correction, the green-to-red fluorescence ratio was calculated. The values for background correction were determined by quantifying the average fluorescence in manually selected cell-free regions of the images. For cells expressing mitochondrially targeted constructs, individual cells were manually segmented, and green-to red fluorescence ratio was determined separately for each cell. For cells expressing

cytosolic constructs, precise determination of cell boundaries was not feasible; therefore, individual regions of interest were placed over spots showing high green and/or red fluorescence.

Mitochondrial respiration

Mitochondrial respiration of adipocytes either derived from the cell lines or the stromal-vascular fraction was determined by measuring oxygen consumption rate (OCR) using the Seahorse XF Cell mito stress test (Agilent Technologies) in the Seahorse Xfe96 Analyzer according to the manufacturer's protocol. Briefly, cells were incubated for 1h with 180 µl Seahorse assay medium containing 1 mM sodium pyruvate, 2 mM glutamine, and 5 mM glucose. For CL-316,243 treatment, cells were washed twice, then incubated briefly with the same medium. Subsequently, the cells were stimulated with 2 µM oligomycin, 1 µM FCCP, and 0.75 µM rotenone/antimycin A (Sigma-Aldrich). The cells are then fixed in 75% ethanol, and the total DNA content was assessed by crystal violet staining. Crystal Violet was dissolved in 10% acetic acid, and the absorption was measured at 590 nm in a Spark 10 M microplate reader (Tecan). The measurements were used to normalize the seahorse values.

Puromycin incorporation assays

Puromycin was added to culture medium at a final concentration of 10 µg/mL and incubated for exactly 10 min. Cells were rinsed with ice-cold PBS and immediately lysed. Western blot analysis was then performed to detect puromycin incorporation into newly synthesized polypeptide chains.

Ribosome isolation

Cells were lysed in a buffer containing 15 mM Tris (pH 7.5), 0.5% NP40, 6 mM $MgCl_2$, 300 mM NaCl, and RiboLock. Lysates were centrifuged at 12,000 × g for 10 min at 4 °C. The resulting supernatant was carefully layered onto a 30% sucrose cushion prepared in 20 mM Tris (pH 7.5), 2 mM $MgCl_2$, and 150 mM KCl, followed by ultracentrifugation at 38,800 rpm for 16 hours using a Beckman Coulter L-100XP ultracentrifuge equipped with a Beckman Coulter 45 Ti rotor. Pelleted ribosomes were washed three times with PBS and resuspended in ribosome elution buffer containing 100 mM KCl, 5 mM $MgCl_2$, 20 mM HEPES (pH 7.6), 1 mM DTT, and 10 mM NH_4Cl. The purified ribosomal fractions were subsequently analyzed by SDS-PAGE and western blotting.

Immunofluorescence staining, western blotting, and qPCR

For analysis of mitochondrial content, mitochondria were stained by adding 150 nM Mito-Tracker Red (Thermo Fischer Scientific) in the suitable growth medium for 30 min at 37 °C. The cells were fixed with 3.7% for 20 min. After washing with PBS, DNA was stained with DAPI. Cover slides were mounted using ProLong Gold Antifade Mountant (Thermo Fischer Scientific). Images were acquired with Microscope: Upright Olympus VS110; Camera Hamamatsu ORCA Flash4.0 V2 2048 x 2048 pixels, software OLYMPUS VS-ASW and Inverted Leica DMI8, CAMERA LEICA DFC365 FX. Images were treated with ImageJ or Fiji.

RNA was extracted using TRIzol reagent according to the standard protocol, and first-strand cDNA was synthesized with the First Strand cDNA Synthesis Kit (Thermo Fischer Scientific) according to the manufacturer's protocol. Real-time quantitative polymerase chain reaction (RT–qPCR) was performed using SYBR Green Universal PCR Master Mix (Thermo Fischer

Scientific) on a CFX Opus 384 (BIO-RAD) system. Gene expression was normalized to the HPRT and 36B housekeeping genes. Mitochondrial DNA (mtDNA) copy number was analyzed from total DNA isolated from cells using the DNeasy Blood & Tissue Kit (Qiagen) according to the manufacturer's instructions. mtDNA was normalized to genomic DNA by RT–qPCR.

Western blotting was performed according to the standard procedure using the indicated antibodies.

Quantification of triglyceride accumulation

Cells were serum-starved for 2 hours in phenol red-free DMEM supplemented with 2% fatty acid-free BSA, stimulated afterwards with 1 μM isoproterenol for 2 hours. The amount of triglycerides was assessed by staining of AdipoRed reagent (Lonza) according to the manufacturer's protocol. Values were normalized to the cells' total DNA content by Hoechst 33342 staining. Oil Red O staining was used to visualize lipid droplets in cells. Briefly, once fully differentiated, cells were fixed with 3.7% paraformaldehyde for 30 min, and Oil Red O solution was added for 1 hour.

Electron microscopy

Sample preparation

Cells were grown on glass-bottom dishes (MatTek) were fixed with 2.5% glutaraldehyde and 2% paraformaldehyde in 0.1 M HEPES buffer, pH 7.3, for 10 minutes at 37°C and later for one hour at RT. The contrast was performed according to the previously published protocol (Bojko et al., 2020) with some minor changes. First, the cells were postfixed with the mixture of 2% osmium tetroxide (Agar Scientific, AGR1023) and 1.5% potassium ferrocyanide (Sigma Aldrich, St. Louis, MO, USA, P3289) in 0.1 M phosphate buffer, pH 7.5, for 1 h. Next, the

samples were rinsed with ddH_2O and subsequently exposed to 1% aqueous thiocarbohydrazide (Sigma Aldrich, St. Louis, MO, USA, #88535) solution for 20 min, washed with ddH_2O, and incubated with an aqueous solution of 1% osmium tetroxide for 45 min at RT. Afterward, cells were rinsed with ddH_2O and incubated overnight in 1% aqueous solution of uranyl acetate at 4 °C. Next day, the cells were rinsed with ddH_2O, incubated with freshly prepared lead aspartate solution for 30 min at 60 °C, then washed with degassed ddH_2O, and dehydrated using graded dilutions of ice-cold ethanol (30, 50, 70, 80, 90, and 2 × 100%) for 5 min each dilution. The samples were infiltrated with Durcupan resin (Sigma Aldrich, St. Louis, MO, USA, #44610), embedded, and cured in a laboratory oven for at least 72 h at 70 °C.

Transmission Electron Microscopy (TEM)

The blocks of resin were cut into thin sections (65 nm) using an Ultracut R ultramicrotome (Leica Microsystems, Vienna, Austria) and collected on formvar-coated copper grids (Agar Scientific, AGS138-1). Grids with sections were examined with a JEM 1400 (JEOL Co., Tokyo, Japan, 2008) TEM microscope, equipped with an 11-megapixel camera MORADA G2 (EMSIS GmbH, Münster, Germany).

Animal experiments

In Copenhagen, mice were housed at the animal facility of the Panum Institute at the University of Copenhagen. The research was monitored by the Institutional Animal Care and Use Committee. Permissions for mouse breeding and experimentation was obtained from the Danish Animal Experiments Inspectorate (permission numbers 2022-15-0202-00162 and 2022-15-0201-01126). In Warsaw, all animal studies were approved by the local institutional animal care and conducted according to the guidelines and state regulations, following approval from the Polish local animal protection authority (I Lokalna Komisja Etyczna, Uchwala Nr.

1646/2024 and Uchwała Nr. 976/2020). Mice were housed at the animal house of the Nencki Institute. All mice were maintained on a 12:12-hour light:dark cycle in ventilated cages at RT and were allowed ad libitum access to water and commercial rodent chow or high-fat diet (HFD; ResearchDiets #D12331) and water at all times. At the time of the experiment, littermate animals were randomly assigned to experimental groups. Body weight gain was monitored every other week.

For blood glucose tolerance tests, mice underwent overnight fasting before receiving an intraperitoneal injection of glucose (2 g/kg). Blood samples were collected from the tail tip and measured directly using Accu-Chek (Roche) test strips. Glucose levels were recorded under both conditions at baseline and at 15, 30, 60, 90, and 120 min post-injection. To induce thermogenesis, mice received intraperitoneal injections of the β-adrenergic agonist CL-316,243 (CL) at a concentration of 1 mg/kg in PBS as indicated in the respective figures for the designated durations. Indirect calorimetry was performed using the Phenomaster system (TSE), where mice were individually housed with unrestricted access to designated food and water. Following at least 5 days of acclimation, metabolic parameters were recorded as indicated for the designated period during the fed state. For the cold challenge test, based on the protocol previously described (Lim et al., 2012), male 8-week-old mice were divided into two groups for 30 °C (thermoneutrality) and 4 °C acclimation. Before exposure at 4 °C, mice were kept at 18 °C for 1 week for adaptation, then exposed for 1 week at 4 °C. Control mice were kept at 24 °C for 1 week for adaptation, then exposed for 1 week at 30 °C. Mice were single-housed in Phenomaster metabolic cages, to which they were adapted at the 18 °C step. Mice were sacrificed for tissue harvesting at the end of the experiment.

Histology

Tissues were collected, fixed in 3.7% paraformaldehyde, or embedded in Optimal Cutting Temperature (OCT) compound. Paraformaldehyde-fixed tissue underwent tissue processing and was then embedded in paraffin. Following embedding and sectioning at 5 μm, tissues were stained with Hematoxylin and Eosin (H&E).

Droplet size quantification from adipose tissue

Adipose tissue images were read and segmented using aicsimageio (Brown et al.) (4.14.0) and Cellpose-SAM (Pachitariu et al., 2025) (v4.0.3), respectively. Before segmentation, each image was preprocessed and summarized into 1 grayscale channel by summing up all 3 RGB channels. Cellpose-SAM was then executed on each preprocessed image with default parameters except for niter=8000, flow_threshold=0.6, and cellprob_threshold=-5. Droplet size quantification was achieved with pyclesperanto (Rigaud et al., 2024) (v0.10.3). Droplets with a size less than 100 pixels were excluded from the analysis, for which the python (v3.10.13) packages polars (v1.31.0), NumPy (Harris et al., 2020) (v1.26.4), matplotlib (Matplotlib, 2007) (v3.10.3), seaborn (Waskom, 2021) (v0.13.2), and scikit-learn (Pedregosa et al., 2011) (v1.4.1) were used. To classify droplets into “BAT” and “WAT” groups, we first modeled the log-scaled area distributions of fat droplets in BAT and WAT control tissues using Kernel Density Estimation (KDE). This produced two KDE functions representing the log-scaled area distributions for each tissue type. The threshold separating BAT and WAT droplets was defined as the area at which the two distributions intersected, and droplets were classified accordingly. After droplet classification, the percentage of BAT area was calculated as the sum of the areas of all BAT droplets divided by the sum of the total segmented area (BAT + WAT droplets), per slide or

sample. In the Warsaw samples, the degree of browning was quantified using ImageJ by calculating the proportion of the image area occupied by multilocular adipocytes relative to the total image area.

Immunofluorescence tissue staining

After defrosting, sections were fixed with 3.7% paraformaldehyde in PBS for 15 min, and then washed 3 times with PBS for 5 min. Sections were blocked with 1% goat serum in 0.3% Triton-5% BSA-PBS solution for 45 min and then incubated with primary antibody against UCP1 (diluted in 0.5% goat serum in 0.3% Triton-5% BSA-PBS solution) for 16 hours. After washing in 0.05% PBS, sections were incubated with fluorescein isothiocyanate (FITC) conjugated antirabbit secondary antibodies diluted in the same solution as the primary antibody at RT for 1 hour. After washing in PBS, DNA was stained with DAPI at RT for 10 min. After mounting with ProLong Diamond Antifade (Molecular Probes). Images were acquired with the Upright Olympus VS110 microscope (Camera Hamamatsu ORCA Flash4.0 V2 2048 x 2048 pixels, software OLYMPUS VS-ASW).

Pull-down of polyubiquitinated proteins by TUBEs (Tandem Ubiquitin Binding Entities 1)

Differentiated adipocytes were lysed in 50 mM Tris-HCl, pH 7.5, 0.15 M NaCl, 1 mM EDTA, 1% NP-40, 10% glycerol, Protease and Phosphatase Cocktail Inhibitor, 50 µM PR619, and 5 mM o-phenanthroline. Total protein content of pre-cleared (Control Agarose) lysate was determined by Pierce BCA Protein Assay Kit, and 20 µl of Agarose-TUBE 2 resin was added to 1 mg of total protein. Reactions were rotated overnight (4˚C), washed three times with 20 mM Tris-HCl, pH 8.0, 0.15 M NaCl, 0.1% Tween-20, and analyzed by SDS-PAGE and immunoblotting.

Quantification and statistical analysis

Statistics

Data were expressed as mean ± S.E.M. Statistical analysis was performed using GraphPad Prism 10 (GraphPad Software, Inc., La Jolla, Ca). Statistical significance was calculated by Mann-Whitney test; ns: nonsignificant; *P < 0.05; **P < 0.01; ***P < 0.001; ****P < 0.0001. Histological analysis of iWAT and BAT was performed in a blinded fashion. For mitochondrial content measurement, about 80 cells were randomly selected per condition.

References:

Bai, Z., Chai, X.-r., Yoon, M.J., Kim, H.-J., Lo, K.A., Zhang, Z.-c., Xu, D., Siang, D.T.C., Walet, A.C.E., and Xu, S.-h. (2017). Dynamic transcriptome changes during adipose tissue energy expenditure reveal critical roles for long noncoding RNA regulators. PLoS biology *15*, e2002176.

Bojko, A., Staniak, K., Czarnecka-Herok, J., Sunderland, P., Dudkowska, M., Śliwińska, M.A., Salmina, K., and Sikora, E. (2020). Improved autophagic flux in escapers from doxorubicin-induced senescence/polyploidy of breast cancer cells. International journal of molecular sciences *21*, 6084.

Brown, E., Toloudis, D., Sherman, J., Swain-Bowden, M., Lambert, T., and Contributors, A. Aicsimageio: Image reading, metadata conversion, and image writing for microscopy images in pure python, 2021. URL https://github com/AllenCellModeling/aicsimageio.

Durinck, S., Spellman, P.T., Birney, E., and Huber, W. (2009). Mapping identifiers for the integration of genomic datasets with the R/Bioconductor package biomaRt. Nature protocols *4*, 1184-1191.

El-Merahbi, R., Viera, J.T., Valdes, A.L., Kolczynska, K., Reuter, S., Löffler, M.C., Erk, M., Ade, C.P., Karwen, T., and Mayer, A.E. (2020). The adrenergic-induced ERK3 pathway drives lipolysis and suppresses energy dissipation. Genes & development *34*, 495-510.

Harris, C.R., Millman, K.J., Van Der Walt, S.J., Gommers, R., Virtanen, P., Cournapeau, D., Wieser, E., Taylor, J., Berg, S., and Smith, N.J. (2020). Array programming with NumPy. nature *585*, 357-362.

Lim, S., Honek, J., Xue, Y., Seki, T., Cao, Z., Andersson, P., Yang, X., Hosaka, K., and Cao, Y. (2012). Cold-induced activation of brown adipose tissue and adipose angiogenesis in mice. Nature protocols *7*, 606-615.

Matplotlib, H.J. (2007). A 2D graphics environment. Comput Sci Eng *9*, 90-95.

Pachitariu, M., Rariden, M., and Stringer, C. (2025). Cellpose-SAM: superhuman generalization for cellular segmentation. bioRxiv, 2025.2004. 2028.651001.

Pedregosa, F., Varoquaux, G., Gramfort, A., Michel, V., Thirion, B., Grisel, O., Blondel, M., Prettenhofer, P., Weiss, R., and Dubourg, V. (2011). Scikit-learn: Machine learning in Python. the Journal of machine Learning research *12*, 2825-2830.

Rigaud, S., Haase, R., Soltwedel, J., Albert, M., and Rajasekhar, P. (2024). clEsperanto/pyclesperanto: 0.16. 0. Zenodo.

Ritchie, M.E., Phipson, B., Wu, D., Hu, Y., Law, C.W., Shi, W., and Smyth, G.K. (2015). limma powers differential expression analyses for RNA-sequencing and microarray studies. Nucleic acids research *43*, e47-e47.

Sustarsic, E.G., Ma, T., Lynes, M.D., Larsen, M., Karavaeva, I., Havelund, J.F., Nielsen, C.H., Jedrychowski, M.P., Moreno-Torres, M., and Lundh, M. (2018). Cardiolipin synthesis in brown and

beige fat mitochondria is essential for systemic energy homeostasis. Cell metabolism *28*, 159-174. e111.
Waskom, M.L. (2021). Seaborn: statistical data visualization. Journal of open source software *6*, 3021.
Wickham, H. (2011). ggplot2. Wiley interdisciplinary reviews: computational statistics *3*, 180-185.